

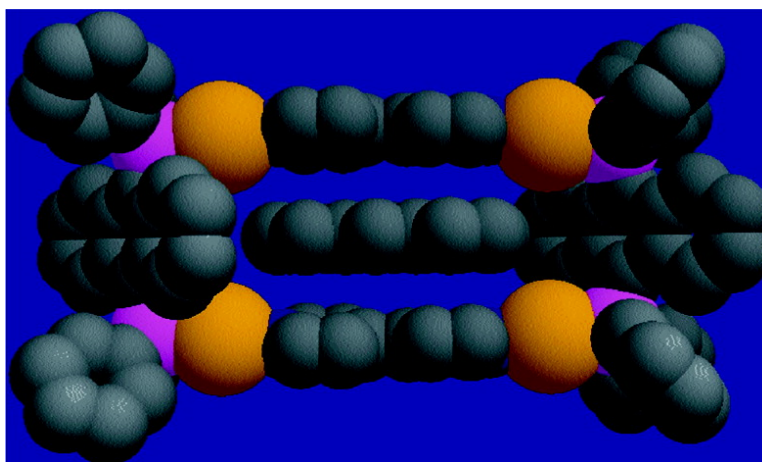
Article

## Self-Assembly and Molecular Recognition of a Luminescent Gold Rectangle

Ronger Lin, John H. K. Yip, Ke Zhang, Lip Lin Koh, Kwok-Yin Wong, and Kam Piu Ho

*J. Am. Chem. Soc.*, **2004**, 126 (48), 15852-15869 • DOI: 10.1021/ja0456508 • Publication Date (Web): 11 November 2004

Downloaded from <http://pubs.acs.org> on April 5, 2009



### More About This Article

Additional resources and features associated with this article are available within the HTML version:

- Supporting Information
- Links to the 5 articles that cite this article, as of the time of this article download
- Access to high resolution figures
- Links to articles and content related to this article
- Copyright permission to reproduce figures and/or text from this article

[View the Full Text HTML](#)

## Self-Assembly and Molecular Recognition of a Luminescent Gold Rectangle

Ronger Lin,<sup>†</sup> John H. K. Yip,<sup>\*†</sup> Ke Zhang,<sup>†</sup> Lip Lin Koh,<sup>†</sup> Kwok-Yin Wong,<sup>‡</sup> and Kam Piu Ho<sup>‡</sup>

Contribution from the Department of Chemistry, The National University of Singapore, 10 Kent Ridge Crescent, 119260, Singapore, and Department of Applied Biology and Chemical Technology, Hong Kong Polytechnic University, Hungghom, Kowloon, Hong Kong SAR, People's Republic of China

Received July 20, 2004; E-mail: chmyiphk@nus.edu.sg

**Abstract:** A luminescent molecular rectangle  $[\text{Au}_4(\mu\text{-PANP})_2(\mu\text{-bipy})_2](\text{OTf})_4$  ( $1 \cdot (\text{OTf})_4$ ) (PANP = 9,10-bis-(diphenylphosphino)anthracene, bipy = 4,4'-bipyridine, X =  $\text{NO}_3^-$  or  $\text{OTf}^-$ ), synthesized from the self-assembly of the molecular "clip"  $\text{Au}_2(\mu\text{-PANP})(\text{OTf})_2$  and bipy, shows a large rectangular cavity of  $7.921(3) \times 16.76(3)$  Å. The electronic absorption and emission spectroscopy, and electrochemistry of the metallacyclophane, have been studied. The  $1^{4+}$  ions are self-assembled into 2D mosaic in the solid state via complementary edge-to-face interactions between the Ph groups.  $^1\text{H}$  NMR titrations ratify the 1:1 complexation between  $1^{4+}$  and various aromatic molecules. Comparing the structures of the inclusion complexes indicates an induced-fit mechanism operating in the binding. The emission of  $1^{4+}$  is quenched upon the guest binding. The binding constants are determined by both  $^1\text{H}$  NMR and fluorescence titrations. Solvophobic and ion-dipole effects are shown to be important in stabilizing the inclusion complexes.

### Introduction

A major facet of host-guest chemistry is to understand molecular recognition, a multitude of processes and interactions that lies at the heart of many biological phenomena.<sup>1</sup> On the practical side, the knowledge gleaned from the studies provides leads to the design of artificial supramolecules that are applicable in advanced technologies such as catalysis, chemical sensing, molecular machinery, and electronics.<sup>2</sup> Traditionally, the field has been dominated by organic molecules, and the host-guest chemistry of receptors such as crown ether,<sup>3</sup> cryptand,<sup>4</sup> and cyclophanes<sup>5</sup> has been studied extensively. Recently, there is a burgeoning interest in the inorganic counterparts of cyclophanes, often known as metallacyclophanes or metallacycles. This class

of compounds is usually synthesized by the coordination-directed self-assembly of transition metal and multitopic ligands.<sup>6</sup> This synthetic methodology has been proved to be very versatile and far-reaching, as based on it a myriad of molecular triangles,<sup>7</sup> squares,<sup>7d,8</sup> rectangles,<sup>8y,9</sup> pentagons,<sup>10</sup> hexagons,<sup>11</sup> macrocycles,<sup>12</sup> polyhedrons, and cages<sup>13,14</sup> have been created. A major advantage of metallacyclophanes over the organic cyclophanes is their modularity that allows control over and fine-tuning of their dimensions, topology, electronic properties, and binding selectivity. Furthermore, it is synthetically straightforward to introduce functional units such as catalytic,<sup>7m,15</sup> luminescent,<sup>7c,d,8n-p,s,t,x,9f,l-n,11b,12e,16</sup> or redox-active centers<sup>8r,16b,17</sup> into the frameworks of the metallacyclophanes. These properties of metallacyclophanes entail their potential applications in advanced materials, and indeed significant progress of engineer-

<sup>†</sup> The National University of Singapore.

<sup>‡</sup> Hong Kong Polytechnic University.

- (1) (a) Cram, D. J. *Angew. Chem., Int. Ed. Engl.* **1988**, *27*, 1009. (b) Lehn, J.-M. *Supramolecular Chemistry: Concepts and Perspectives*; VCH: Weinheim, 1995. (c) *Comprehensive Supramolecular Chemistry*; Lehn, J.-M., Chair Ed.; Atwood, J. L., Davis, J. E. D., MacNicol, D. D., Vogtle, F., Exec. Eds.; Pergamon: Oxford, UK, 1996; Vols. 1-11. (d) Philp, D.; Stoddart, J. F. *Angew. Chem., Int. Ed. Engl.* **1996**, *35*, 1154.
- (2) (a) Lehn, J.-M. *Science* **2002**, *295*, 2400. (b) Reinhoudt, D. N.; Crego-Calama, M. *Science* **2002**, *295*, 2403. (c) Prins, L. J.; Reinhoudt, D. N.; Timmerman, P. *Angew. Chem., Int. Ed.* **2001**, *40*, 2382. (d) Caulder, D. L.; Raymond, K. N. *Acc. Chem. Res.* **1999**, *32*, 975. (e) Collier, C. P.; Matternsteig, G.; Wong, E. W.; Luo, Y.; Beverly, K.; Sampaio, J.; Raymo, F. M.; Stoddart, J. F.; Heath, J. R. *Science* **2000**, *289*, 1172. (f) Balzani, V.; Credi, A.; Venturi, M. *Chem.-Eur. J.* **2002**, *8*, 5524. (g) Mobian, P.; Kern, J.-M.; Sauvage, J.-P. *Angew. Chem., Int. Ed.* **2004**, *43*, 2392. (h) Gale, P. A.; Anzenbacher, P., Jr.; Sessler, J. L. *Coord. Chem. Rev.* **2001**, *222*, 57. (i) Marty, M.; Clyde-Watson, Z.; Twyman, L. J.; Nakash, M.; Sanders, J. K. M. *J. Chem. Soc., Chem. Commun.* **1998**, 2265. (j) Schenning, A. P. H.; Lutje-Seplberg, J. H.; Hubert, D. H. W.; Feiters, M. C.; Nolte, R. J. M. *Chem.-Eur. J.* **1998**, *4*, 871.
- (3) Pedersen, C. J. *Angew. Chem., Int. Ed. Engl.* **1988**, *27*, 1021.
- (4) Lehn, J.-M. *Angew. Chem., Int. Ed. Engl.* **1988**, *27*, 89.
- (5) Diederich, F. *Cyclophanes*; Royal Society of Chemistry: Cambridge, 1991.

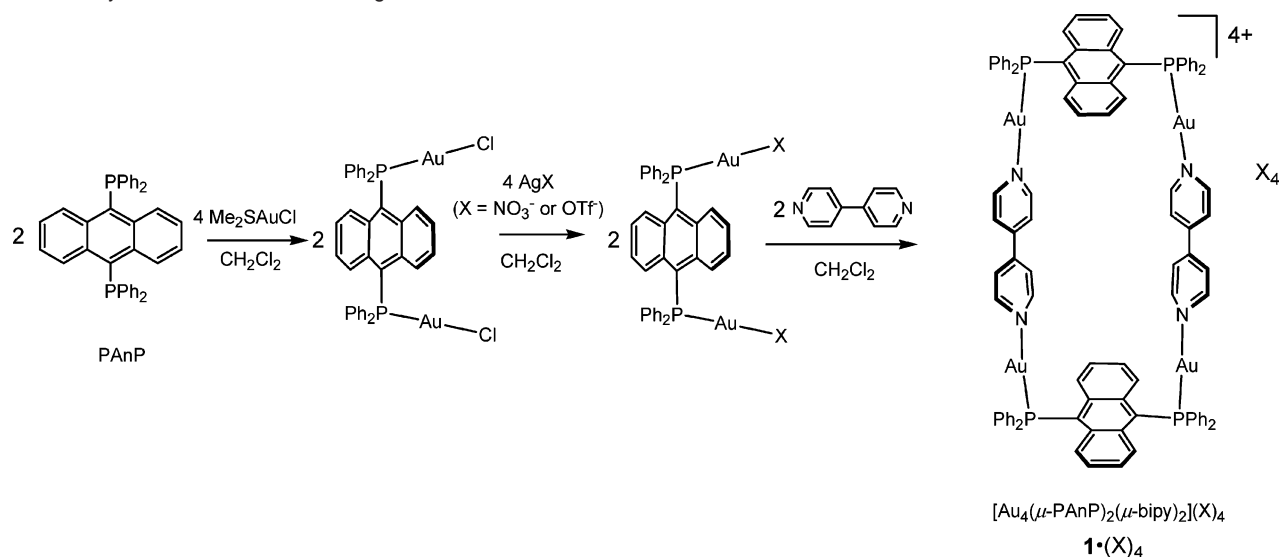
- (6) For reviews, see: (a) Fujita, M. *Chem. Soc. Rev.* **1998**, *27*, 417. (b) Fujita, M. *Acc. Chem. Res.* **1999**, *32*, 53. (c) Leininger, S.; Olenyuk, B.; Stang, P. J. *Chem. Rev.* **2000**, *100*, 853. (d) Seidel, S. R.; Stang, P. J. *Acc. Chem. Res.* **2002**, *35*, 972. (e) Caulder, D. L.; Raymond, K. N. *J. Chem. Soc., Dalton Trans.* **1999**, 1185. (f) Holliday, B. J.; Mirkin, C. A. *Angew. Chem., Int. Ed.* **2001**, *40*, 2022. (g) Würthner, F.; You, C. C.; Saha-Möller, C. R. *Chem. Soc. Rev.* **2004**, 133. (h) Swieggers, G. F.; Malefetse, T. J. *Coord. Chem. Rev.* **2002**, *225*, 91. (i) Cotton, F. A.; Lin, C.; Murillo, C. A. *Acc. Chem. Res.* **2001**, *34*, 759. (j) Uller, E.; Demleitner, I.; Bernt, I.; Saalfrank, R. W. Synergistic Effect of Serendipity and Rational Design in Supramolecular Chemistry. In *Structure and Bonding*; Fujita, M., Ed.; Springer: Berlin, 2000; Vol. 96, p 149. (k) Baxter, P. N. W.; Lehn, J.-M.; Baum, G.; Fenske, D. *Chem.-Eur. J.* **1999**, *5*, 102. (l) Chambron, J.-C.; Dietrich-Buchecker, C.; Sauvage, J.-P. Transition Metals as Assembling and Templating Species. In *Comprehensive Supramolecular Chemistry*; Lehn, J.-M., Chair, E., Atwood, J. L., Davis, J. E. D., MacNicol, D. D., Vogtle, F., Eds.; Pergamon Press: Oxford, 1996; Vol. 9, Chapter 2, p 43. (m) Baxter, P. N. W. Metal Ion Directed Assembly of Complex Molecular Architectures and Nanostructures. In *Comprehensive Supramolecular Chemistry*; Lehn, J.-M., Chair, E., Atwood, J. L., Davis, J. E. D., MacNicol, D. D., Vogtle, F., Eds.; Pergamon Press: Oxford, 1996; Vol. 9, Chapter 5, p 165.

ing metallacyclophanes into luminescent and electrochemical sensors, molecular sieves, and catalysts has been made in recent years.<sup>15–18</sup> Aside from the practical aspects, study of the thermodynamics and kinetics of the self-assembly of metallacyclophanes would provide important insights into the evolution and emergence of complex structures.<sup>14,19</sup>

The substrate-binding ability of metallacycles was first demonstrated in the complexation between 1,4-diazabicyclo-[2,2,2]octane and a cofacial dicopper(II) macrocycle.<sup>20</sup> Fujita et al. first showed the self-assembly of the molecular squares

- (7) (a) Fujita, M. *J. Synth. Org. Chem. Jpn.* **1996**, *54*, 953. (b) Fujita, M.; Sasaki, O.; Mitsuhashi, T.; Fujita, T.; Yazaki, J.; Yamaguchi, K.; Ohura, K. *J. Chem. Soc., Chem. Commun.* **1996**, 1535. (c) Sun, S.-S.; Lees, A. J. *Organometallics* **2002**, *21*, 39. (d) Sun, S.-S.; Lees, A. J. *J. Am. Chem. Soc.* **2000**, *122*, 8956. (e) Kryschenko, Y. K.; Seidel, S. R.; Arif, A. M.; Stang, P. J. *J. Am. Chem. Soc.* **2003**, *125*, 5193. (f) Schweiger, M.; Seidel, S. R.; Arif, A. M.; Stang, P. J. *Inorg. Chem.* **2002**, *41*, 2556. (g) Hall, J.; Loeb, S. J.; Shimizu, G. H. K.; Yap, G. P. A. *Angew. Chem., Int. Ed.* **1998**, *37*, 121. (h) Lee, S. B.; Hwang, S. G.; Chung, D. S.; Yun, H.; Hong, J.-I. *Tetrahedron Lett.* **1998**, *39*, 873. (i) Schnebeck, R.-D.; Randaccio, L.; Zangrando, E.; Lippert, B. *Angew. Chem., Int. Ed.* **1998**, *37*, 119. (j) Lai, S.-W.; Chan, M. C.-W.; Peng, S.-M.; Che, C.-M. *Angew. Chem., Int. Ed.* **1999**, *38*, 669. (k) Baker, A. T.; Crass, J. K.; Maniska, M.; Craig, D. C. *Inorg. Chim. Acta* **1995**, *230*, 225. (l) Cotton, F. A.; Daniels, L. M.; Lin, C.; Murillo, C. A. *J. Am. Chem. Soc.* **1999**, *121*, 4538. (m) Lee, S. J.; Hu, A.; Lin, W. *J. Am. Chem. Soc.* **2002**, *124*, 12948. (n) Qin, Z.; Jennings, M. C.; Puddephatt, R. J. *Inorg. Chem.* **2002**, *41*, 3967. (o) Jennings, M. C.; Puddephatt, R. J. *J. Chem. Soc., Chem. Commun.* **2001**, 2676.
- (8) (a) Strickland, P. M.; Volcko, E. J.; Verkade, J. G. *J. Am. Chem. Soc.* **1983**, *105*, 2494. (b) Fujita, M.; Yazaki, J.; Ogura, K. *J. Am. Chem. Soc.* **1990**, *112*, 5645. (c) Fujita, M.; Yazaki, J.; Ogura, K. *Tetrahedron Lett.* **1991**, *32*, 5589. (d) Stang, P. J.; Cao, D. H. *J. Am. Chem. Soc.* **1994**, *116*, 4981. (e) Stang, P. J.; Cao, D. H.; Saito, S.; Arif, A. M. *J. Am. Chem. Soc.* **1995**, *117*, 6273. (f) Stang, P. J.; Olenyuk, B. *Angew. Chem., Int. Ed. Engl.* **1996**, *35*, 732. (g) Olenyuk, B.; Whiteford, J. A.; Stang, P. J. *J. Am. Chem. Soc.* **1996**, *118*, 8221. (h) Stang, P. J.; Olenyuk, B. *Angew. Chem., Int. Ed. Engl.* **1996**, *35*, 732. (i) Müller, C.; Whiteford, J. A.; Stang, P. J. *J. Am. Chem. Soc.* **1998**, *120*, 9827. (j) Stang, P. J.; Cao, D. H.; Chen, K.; Gray, G. M.; Muddiman, D. C.; Smith, R. D. *J. Am. Chem. Soc.* **1997**, *119*, 5163. (k) Manna, J.; Kuehl, C. J.; Whiteford, J. A.; Stang, P. J.; Muddiman, D. C.; Hofstadler, S. A.; Smith, R. D. *J. Am. Chem. Soc.* **1997**, *119*, 11611. (l) Rauter, H.; Hillgeris, E. C.; Lippert, B. *J. Chem. Soc., Chem. Commun.* **1992**, 1385. (m) Rauter, H.; Hillgeris, E. C.; Erxleben, A.; Lippert, B. *J. Am. Chem. Soc.* **1994**, *116*, 616. (n) Slone, R. V.; Hupp, J. T.; Stern, C. L.; Albrecht-Schmitt, T. E. *Inorg. Chem.* **1996**, *35*, 4096. (o) Slone, R. V.; Hupp, J. T. *Inorg. Chem.* **1997**, *36*, 5422. (p) Slone, R. V.; Yoon, D. I.; Calhoun, R. M.; Hupp, J. T. *J. Am. Chem. Soc.* **1995**, *117*, 11813. (q) Sun, S.-S.; Stern, C. L.; Nguyen, S. T.; Hupp, J. T. *J. Am. Chem. Soc.* **2004**, *126*, 6314. (r) You, C.-C.; Würthner, F. *J. Am. Chem. Soc.* **2003**, *125*, 9716. (s) Sautter, A.; Schmid, D. G.; Jung, G.; Würthner, F. *J. Am. Chem. Soc.* **2001**, *123*, 5424. (t) Drain, C. M.; Lehn, J.-M. *J. Chem. Soc., Chem. Commun.* **1994**, 2313. (u) Chi, X.; Guerin, A. J.; Haycock, R. A.; Hunter, C. A.; Sarson, L. D. *J. Chem. Soc., Chem. Commun.* **1995**, 2567. (v) Lee, S. J.; Lin, W. *J. Am. Chem. Soc.* **2002**, *124*, 4554. (w) Cotton, F. A.; Lin, C.; Murillo, C. A. *Inorg. Chem.* **2001**, *40*, 478. (x) Manimaran, B.; Thanasekaran, P.; Rajendran, T.; Liao, R.-T.; Liu, Y.-H.; Lee, G.-H.; Peng, S.-M.; Rajagopal, S.; Lu, K.-L. *Inorg. Chem.* **2003**, *42*, 4795. (y) Jeong, K.-S.; Cho, Y. L.; Chang, S.-Y.; Park, T.-Y.; Song, J. U. *J. Org. Chem.* **1999**, *64*, 9459.
- (9) (a) Fujita, M.; Ibukuro, F.; Yamaguchi, K.; Ogura, K. *J. Am. Chem. Soc.* **1995**, *117*, 4175. (b) Fujita, M.; Aoyagi, M.; Ibukuro, F.; Ogura, K.; Yamaguchi, K. *J. Am. Chem. Soc.* **1998**, *120*, 611. (c) Yan, H.; Suss-Fink, G.; Neels, A.; Stoekli-Evans, H. *J. Chem. Soc., Dalton Trans.* **1997**, 4345. (d) Benkstein, K. D.; Hupp, J. T.; Stern, C. L. *Inorg. Chem.* **1998**, *37*, 5404. (e) Benkstein, K. D.; Hupp, J. T.; Stern, C. L. *J. Am. Chem. Soc.* **1998**, *120*, 12982. (f) Benkstein, K. D.; Hupp, J. T.; Stern, C. L. *Angew. Chem., Int. Ed.* **2000**, *39*, 2891. (g) Kuehl, C. J.; Huang, S. D.; Stang, P. J. *J. Am. Chem. Soc.* **2001**, *123*, 9634. (h) Kuehl, C. J.; Mayne, C. L.; Arif, A. M.; Stang, P. J. *Org. Lett.* **2000**, *2*, 3727. (i) Woessner, S. M.; Helms, J. B.; Shen, Y.; Sullivan, B. P. *Inorg. Chem.* **1998**, *37*, 5406. (j) Sommer, R. D.; Rheingold, A. L.; Goshe, A. J.; Bosnich, B. *J. Am. Chem. Soc.* **2001**, *123*, 3940. (k) Constable, E. C.; Schofield, E. J. *J. Chem. Soc., Chem. Commun.* **1998**, 403. (l) Rajendran, T.; Manimaran, B.; Lee, F.-Y.; Lee, G.-H.; Peng, S.-M.; Wang, C. M.; Lu, K.-L. *Inorg. Chem.* **2000**, *39*, 2016. (m) Manimaran, B.; Thanasekaran, P.; Rajendran, T.; Lin, R.-J.; Chang, I.-J.; Lee, G.-H.; Peng, S.-M.; Rajagopal, S.; Lu, K.-L. *Inorg. Chem.* **2002**, *41*, 5323. (n) Rajendran, T.; Manimaran, B.; Liao, R.-T.; Lin, R.-J.; Thanasekaran, P.; Lee, G.-H.; Peng, S.-M.; Liu, Y.-H.; Chang, I.-J.; Rajagopal, S.; Lu, K.-L. *Inorg. Chem.* **2003**, *42*, 6388. (o) Bera, J. K.; Campos-Fernandez, C. S.; Rodolphe, C.; Dunbar, K. R. *J. Chem. Soc., Chem. Commun.* **2002**, 2536. (p) Suzuki, H.; Tajima, N.; Tatsumi, K.; Yamamoto, Y. *J. Chem. Soc., Chem. Commun.* **2000**, 1801.
- (10) (a) Hasenknopf, B.; Lehn, J.-M.; Baum, G.; Kneisel, B. O.; Fenske, D. *Angew. Chem., Int. Ed. Engl.* **1996**, *35*, 1838. (b) Campos-Fernandez, C. S.; Clerac, R.; Koomen, J. M.; Russell, D. H.; Dunbar, K. R. *J. Am. Chem. Soc.* **2001**, *123*, 773.
- [M<sub>4</sub>(en)<sub>4</sub>(u-bipy)<sub>4</sub>](NO<sub>3</sub>)<sub>8</sub> (M = Pd<sup>II</sup>, Pt<sup>II</sup>, en = 1,2-diaminoethane, bipy = 4,4'-bipyridine), which bind to neutral and anionic aromatic molecules.<sup>8b,c</sup> Later studies showed that binuclear Pd<sup>II</sup>-macrocycles which contain flexible and electron-deficient linkers could exhibit shape selectivity and higher affinity for electron-rich aromatics.<sup>21</sup> The substrate-binding properties of metalla-
- (11) (a) Stang, P. J.; Persky, N.; Manna, J. *J. Am. Chem. Soc.* **1997**, *119*, 4777. (b) Lai, S. W.; Cheung, K. K.; Chan, M. C.; Che, C. M. *Angew. Chem., Int. Ed.* **1998**, *37*, 182. (c) Mamula, O.; von Zelewsky, A.; Bernardinelli, G. *Angew. Chem., Int. Ed.* **1998**, *37*, 289. (d) Matsumoto, N.; Motoda, Y.; Matsuo, T.; Nakashima, T.; Re, N.; Dahan, F.; Tuchagues, J.-P. *Inorg. Chem.* **1999**, *38*, 1165. (e) Mingos, D. M. P.; Yau, J.; Menzer, S.; Williams, D. J. *Angew. Chem., Int. Ed. Engl.* **1995**, *34*, 1894. (f) Jiang, H.; Lin, W. *J. Am. Chem. Soc.* **2003**, *125*, 8084. (g) Cho, Y. L.; Uh, H.; Chang, S.-Y.; Chang, H.-Y.; Choi, M.-G.; Shin, I.; Jeong, K.-S. *J. Am. Chem. Soc.* **2001**, *123*, 1258.
- (12) (a) Fujita, M.; Ibukuro, F.; Hagihara, H.; Ogura, K. *J. Nature* **1994**, *367*, 720. (b) Liu, X.; Stern, C. L.; Mirkin, C. A. *Organometallics* **2002**, *21*, 1017. (c) Eisenberg, A. H.; Ovchinnikov, M. V.; Mirkin, C. A. *J. Am. Chem. Soc.* **2003**, *125*, 2836. (d) Holliday, B. J.; Ulmann, P. A.; Mirkin, C. A.; Stern, C. L.; Zakharov, L. N.; Rheingold, A. L. *Organometallics* **2004**, *23*, 1671. (e) Yip, J. H. K.; Prabhavathy, J. *Angew. Chem., Int. Ed.* **2001**, *40*, 2159. (f) Su, C.-Y.; Cai, Y.-P.; Chen, C.-L.; Smith, M. D.; Kaim, W.; zur Loye, H.-C. *J. Am. Chem. Soc.* **2003**, *125*, 8595. (g) Jiang, H.; Lin, W. *J. Am. Chem. Soc.* **2004**, *126*, 7426.
- (13) (a) Fujita, M.; Oguro, D.; Miyazawa, M.; Oka, H.; Yamaguchi, K.; Ogura, K. *Nature* **1995**, *378*, 469. (b) Olenyuk, B.; Whiteford, J. A.; Fechtenkötter, A.; Stang, P. J. *Nature* **1999**, *398*, 796. (c) Takeda, N.; Umamoto, K.; Yamaguchi, K.; Fujita, M. *Nature* **1999**, *398*, 794. (d) Xu, J.; Stack, T. D. P.; Raymond, K. N. *Inorg. Chem.* **1992**, *31*, 4903. (e) Beissel, T.; Powers, R. E.; Raymond, K. N. *Angew. Chem., Int. Ed. Engl.* **1996**, *35*, 1084. (f) Saalfrank, R. W.; Bernt, I.; Uller, E.; Hampel, F. *Angew. Chem., Int. Ed.* **2000**, *39*, 1239. (g) Jacopozzi, P.; Dalcanele, E. *Angew. Chem., Int. Ed. Engl.* **1997**, *36*, 613. (h) Fochi, F.; Jacopozzi, P.; Wegelius, E.; Rissanen, K.; Cozzini, P.; Marastoni, E.; Fiscicor, E.; Manini, P.; Fokkens, R.; Dalcanele, E. *J. Am. Chem. Soc.* **2001**, *123*, 7539. (i) Stulz, E.; Scott, S. M.; Bond, A. D.; Teat, S. J.; Sanders, J. K. M. *Chem.-Eur. J.* **2003**, *24*, 6039. (j) Radhakrishnan, U.; Schweiger, M.; Stang, P. J. *Org. Lett.* **2001**, *3*, 3141. (k) Fiedler, D.; Pagliero, D.; Brumaghim, J. L.; Bergman, R. G.; Raymond, K. N. *Inorg. Chem.* **2004**, *43*, 846. (l) Mukherjee, P. S.; Das, N.; Stang, P. J. *J. Org. Chem.* **2004**, *69*, 3526. (m) Hiraoka, S.; Fujita, M. *J. Am. Chem. Soc.* **1999**, *121*, 10239. (n) Fujita, M.; Yu, S. Y.; Kusukawa, T.; Funaki, H.; Ogura, K.; Yamaguchi, K. *Angew. Chem., Int. Ed.* **1998**, *37*, 2082. (o) Contakes, S. M.; Kuhlman, M. L.; Ramesh, M.; Wilson, S. R.; Rauchfuss, T. B. *Proc. Natl. Acad. Sci. U.S.A.* **2002**, *99*, 4889. (p) Perkins, D. F.; Lindoy, L. F.; Meehan, G. V.; Turner, P. J. *J. Chem. Soc., Chem. Commun.* **2004**, 152.
- (14) Davis, A. V.; Yeh, R. M.; Raymond, K. N. *Proc. Natl. Acad. Sci. U.S.A.* **2002**, *99*, 4793.
- (15) (a) Sanders, J. K. M. *Chem.-Eur. J.* **1998**, *4*, 1378. (b) Brisig, B.; Sanders, J. K. M.; Otto, S. *Angew. Chem., Int. Ed.* **2003**, *42*, 1270. (c) Merlau, M. L.; Mejia, M. D. P.; Nguyen, S. T.; Hupp, J. T. *Angew. Chem., Int. Ed.* **2001**, *40*, 4239. (d) Morris, G. A.; Nguyen, S. T.; Hupp, J. T. *J. Mol. Catal. A* **2001**, *174*, 15. (e) Gianneschi, N. C.; Bertin, P. A.; Nguyen, S. T.; Mirkin, C. A.; Zakharov, L. N.; Rheingold, A. L. *J. Am. Chem. Soc.* **2003**, *125*, 10508.
- (16) (a) Tzeng, B. C.; Lo, W. C.; Che, C. M.; Peng, S. M. *J. Chem. Soc., Chem. Commun.* **1996**, 181. (b) Sun, S.-S.; Anspach, J. A.; Lees, A. J.; Zavali, P. Y. *Organometallics* **2002**, *21*, 685. (c) Fan, J.; Whiteford, J. A.; Olenyuk, B.; Levin, M. D.; Stang, P. J.; Fleischer, E. B. *J. Am. Chem. Soc.* **1999**, *121*, 2741. (d) Holliday, B. J.; Farrell, J. R.; Mirkin, C. A.; Lam, K.-C.; Rheingold, A. L. *J. Am. Chem. Soc.* **1999**, *121*, 6316. (e) Slone, R. S.; Benkstein, K. D.; Bélanger, S.; Hupp, J. T.; Guzei, I. A.; Rheingold, A. L. *Coord. Chem. Rev.* **1998**, *171*, 221. (f) Würthner, F.; Sautter, A. *Org. Biomol. Chem.* **2003**, *1*, 240.
- (17) (a) Stang, P. J.; Cao, D. H.; Chen, K.; Gray, G. M.; Muddiman, D. C.; Smith, R. D. *J. Am. Chem. Soc.* **1997**, *119*, 5163. (b) Cotton, F. A.; Daniels, L. M.; Lin, C.; Murillo, C. A. *J. Am. Chem. Soc.* **1999**, *121*, 4538. (c) Würthner, F.; Sautter, A. *J. Chem. Soc., Chem. Commun.* **2000**, 445. (d) Würthner, F.; Sautter, A.; Schmid, D.; Weber, A. *Chem.-Eur. J.* **2001**, *7*, 894. (e) Sun, S.-S.; Lees, A. J. *Inorg. Chem.* **2001**, *40*, 3154. (f) Sun, S.-S.; Anspach, J. A.; Lees, A. J. *Inorg. Chem.* **2002**, *41*, 1862. (g) Splan, K. E.; Keefew, M. H.; Massari, A. M.; Walters, K. A.; Hupp, J. T. *Inorg. Chem.* **2002**, *41*, 619.
- (18) (a) Dinolfo, P. H.; Hupp, J. T. *Chem. Mater.* **2001**, *13*, 3113. (b) Nguyen, S. B. T.; Gin, D. L.; Hupp, J. T.; Zhang, X. *Proc. Natl. Acad. Sci. U.S.A.* **2001**, *98*, 11849. (c) Sun, S.-S.; Lees, A. J. *Coord. Chem. Rev.* **2002**, *230*, 170. (d) Sun, S.-S.; Anspach, J. A.; Lees, A. J.; Zavali, P. Y. *Organometallics* **2002**, *21*, 685. (e) Resendiz, M. J. E.; Noveron, J. C.; Disteldorf, H.; Fischer, S.; Stang, P. J. *Org. Lett.* **2004**, *6*, 651. (f) Lee, S. J.; Lin, W. *J. Am. Chem. Soc.* **2002**, *124*, 4554. (g) Hua, J.; Lin, W. *Org. Lett.* **2004**, *6*, 861. (h) Keefe, M. H.; Slone, R. V.; Hupp, J. T.; Czaplowski, K. F.; Snurr, R. Q.; Stern, C. L. *Langmuir* **2000**, *16*, 3964.
- (19) (a) Hasenknopf, B.; Lehn, J.-M.; Boumediene, N.; Dupont-Gervais, A.; Van Dorsselaer, A.; Kneisel, B.; Fenske, D. *Angew. Chem., Int. Ed.* **1998**, *37*, 3265. (b) Levin, M. J.; Stang, P. J. *J. Am. Chem. Soc.* **2000**, *122*, 7428. (c) Kersting, B.; Meyer, M.; Powers, R. E.; Raymond, K. N. *J. Am. Chem. Soc.* **1996**, *118*, 7221.
- (20) Maverick, A. W.; Klavetter, F. E. *Inorg. Chem.* **1984**, *23*, 4129.

Scheme 1. Synthesis of the Gold Rectangle



cycles of  $\text{Zn}^{\text{II}}$ ,<sup>22</sup>  $\text{Ru}^{\text{II}}$ ,<sup>23</sup>  $\text{Pd}^{\text{II}}$ ,<sup>8i,9j,24</sup>  $\text{Pt}^{\text{II}}$ ,<sup>8i,k,24,25</sup>  $\text{Rh}^{\text{I}}$ ,<sup>16d</sup>  $\text{Re}^{\text{I}}$ ,<sup>7d,8o,9e</sup> and  $\text{Os}^{\text{VI}}$ <sup>26</sup> were studied. The metallacycles form inclusion complexes with guests as diverse as substituted benzenes,<sup>7d,8b,c,11g,18d,21–23</sup> anthracenes,<sup>9j,22</sup> square planar  $\text{Pd}^{\text{II}}$  and  $\text{Pt}^{\text{II}}$ , and metalloporphyrin complexes.<sup>8o,9e</sup> The binding invokes  $\pi$ – $\pi$  interactions between the aromatic rings of the hosts and guests,<sup>9j,11g,22</sup> but, in some cases, other interactions such as hydrogen bonds,<sup>8y,26</sup> metal–ligand coordination,<sup>8i,25b</sup> and metal–metal bonds<sup>9j</sup> are also involved. Metallacyclophanes whose luminescence is responsive to the binding of the substrate are of special interest because of the potential applications of the compounds in chemical sensing. Examples of this class of compounds include the molecular rectangles  $[\text{M}_4(\text{CO})_{12}(\mu\text{-bipy})(\text{bipm})_2]$  ( $\text{M} = \text{Mn}^{\text{I}}$  or  $\text{Re}^{\text{I}}$ ),<sup>9d,e,f</sup> a  $\text{Rh}^{\text{I}}$ -cyclophane,<sup>16d</sup> and various  $\text{Re}^{\text{I}}$ ,<sup>7d,8o,16e,18f</sup>  $\text{Re}^{\text{I}}\text{Pd}^{\text{II}}$ ,<sup>18d</sup> and  $\text{Ru}^{\text{II}}$  squares,<sup>23</sup> and  $\text{Re}^{\text{I}}$  and  $\text{Ru}^{\text{II}}$  triangles.<sup>7d,23</sup>

Stereoelectronic complementarity<sup>27</sup> between binding partners and preorganization of the binding site<sup>28</sup> are pertinent to the selectivity and strength of host–guest binding. In this regard, molecular rectangles with extended  $\pi$ -surface should be able to host planar aromatic compounds. Molecular rectangles<sup>8y,9</sup> are less common than molecular squares. Among the early reported molecular rectangles are binuclear  $\text{Pd}^{\text{II}}$  complexes which can be assembled into [2]catenanes.<sup>9a,b</sup> Other examples include  $[\text{M}_4(\text{CO})_{12}(\mu\text{-bipy})(\text{bipm})_2]$  ( $\text{M} = \text{Mn}^{\text{I}}$  and  $\text{Re}^{\text{I}}$ ),<sup>9d,e,f</sup>  $[\text{Pt}_4(\text{PET}_3)_8(\mu\text{-anth}^{2-})_2(\mu\text{-L})]^{4+}$  ( $\text{anth} = \text{anthracene-1,8-diyl}$ ,  $\text{L} = \text{bipy}$ , 1,4-bis(4-ethynylpyridyl)benzene, 2,5-bis(4-ethynylpyridyl)furan or bpe),<sup>9g,h</sup> and rectangles bearing cofacial terpyridyl  $\text{Pd}^{\text{II}}$  complexes.<sup>9j</sup>

Described in this paper are the synthesis, spectroscopy, electrochemistry, solid-state self-assembly, and host–guest chemistry of a luminescent gold rectangle. The present work stemmed from our recent studies of the ligand 9,10-bis(diphenylphosphino)anthracene (PAnP) (Scheme 1).<sup>12e</sup> The ligand, containing a chromophoric anthracene, can impart luminescence to its metal complexes, as exemplified by the gold ring  $[\text{Au}_3(\mu\text{-PAnP})_3\text{ClO}_4](\text{ClO}_4)_2$  which displays intense  $\pi\pi^*$  fluorescence in solution.<sup>12e</sup> Another special feature of PAnP is the adjustable bite distance between the two  $\text{PPh}_2$  donor groups, which is an attribute of the flexible anthracenyl backbone. Our study showed that the two  $\text{P–Au–X}$  units of the binuclear  $\text{Au}_2(\mu\text{-PAnP})\text{X}_2$  ( $\text{X} = \text{Cl}$  and  $\text{Br}$ ) are syn-oriented and widely separated ( $d_{\text{Au–Au}} = 9.154(2)\text{\AA}$ ).<sup>29</sup> This conformation gives the complex a U-shape geometry and an approximate  $C_{2v}$  symmetry, which invites the application of the  $[\text{Au}_2(\mu\text{-PAnP})]^{2+}$  unit as a molecular “clip” in assembling the molecular rectangles. The idea of using a molecular “clip” in assembling metallacycles was illustrated by the recent work of Stang in which the organoplatinum  $[\text{Pt}_2(\mu\text{-anth}^{2-})(\text{OTf})_2]$  clip was used in constructing molecular rectangles  $[\text{Pt}_4(\text{PET}_3)_8(\mu\text{-anth}^{2-})_2(\mu\text{-L})_2](\text{PF}_6)_4$ , cages, and trigonal prisms.<sup>9g,h,30</sup> Rheingold and Bosnich also demonstrated that a molecular cleft comprising cofacial terpyridyl  $\text{Pd}^{\text{II}}$  complexes can combine with bipy to form molecular rectangle and trigonal prisms with large cavity.<sup>9j,31</sup> The well-known propensity<sup>32</sup> of gold(I) for linear coordination geometry has been exploited in constructing metallacycles and catenanes.<sup>33</sup> As shown in the work of Puddephatt, coupling the digold(I) complexes  $[\text{Au}_2(\mu\text{-Ph}_2\text{P}(\text{CH}_2)_n\text{-PPh}_2)(\text{CF}_3\text{CO}_2)_2]$  ( $n = 1, 3, 5$ ) with the ditopic diisocyanobenzene, bipy or bpe ( $\text{L}'$ ) gives rise to the metallacycles  $[\text{Au}_4(\mu\text{-}$

(21) Fujita, M.; Nagao, S.; Ilida, M.; Ogata, K.; Ogura, K. *J. Am. Chem. Soc.* **1993**, *115*, 1574.

(22) Houghton, M. A.; Bilyk, A.; Harding, M. M.; Turner, P.; Hambley, T. W. *J. Chem. Soc., Dalton Trans.* **1997**, 2725.

(23) Xu, D.; Hong, B. *Angew. Chem., Int. Ed.* **2000**, *39*, 1826.

(24) Whiteford, J. A.; Lu, C. V.; Stang, P. J. *J. Am. Chem. Soc.* **1997**, *119*, 2524.

(25) (a) Stang, P. J.; Chen, K.; Arif, A. M. *J. Am. Chem. Soc.* **1995**, *117*, 8793. (b) Whiteford, J. A.; Stang, P. J.; Huang, S. D. *Inorg. Chem.* **1998**, *37*, 5595.

(26) (a) Jeong, K.-S.; Cho, Y. L.; Song, J. U.; Chang, H.-Y.; Choi, M.-G. *J. Am. Chem. Soc.* **1998**, *120*, 10982. (b) Chang, S.-Y.; Jeong, K.-S. *J. Org. Chem.* **2003**, *68*, 4014. (c) Jeong, K.-S.; Choi, J.-S.; Chang, S.-Y.; Chang, H.-Y. *Angew. Chem., Int. Ed.* **2000**, *39*, 1692.

(27) Reference 5, p 61.

(28) Cram, D. J. *Angew. Chem., Int. Ed. Engl.* **1986**, *25*, 1039.

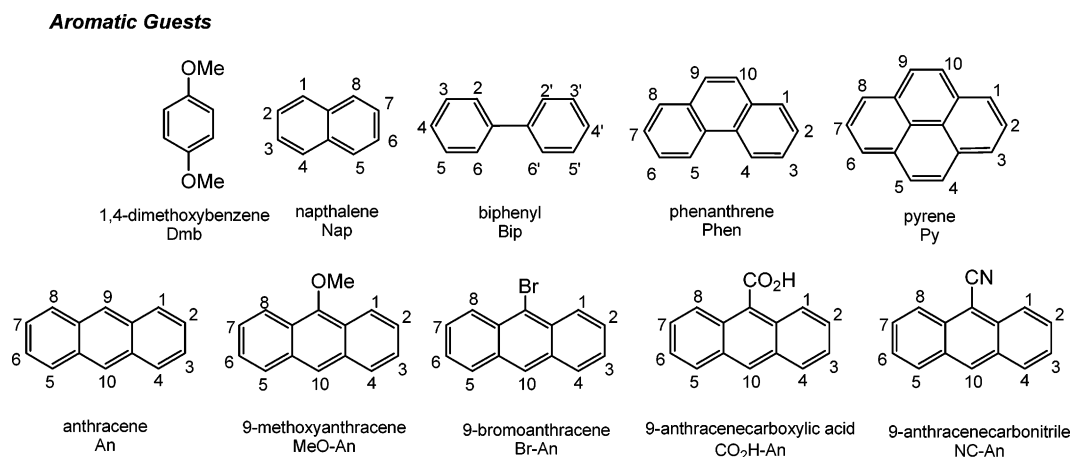
(29) Zhang, K.; Prabhavathy, J.; Yip, J. H. K.; Koh, L. L.; Tan, G. K.; Vittal, J. J. *J. Am. Chem. Soc.* **2003**, *125*, 8452.

(30) (a) Mukherjee, P. S.; Das, N.; Kryschenko, Y. K.; Arif, A. M.; Stang, P. J. *J. Am. Chem. Soc.* **2004**, *126*, 2464. (b) Kryschenko, Y. K.; Seidel, S. R.; Muddiman, D. C.; Nepomuceno, A. I.; Stang, P. J. *J. Am. Chem. Soc.* **2003**, *125*, 9647. (c) Das, N.; Mukherjee, P. S.; Arif, A. M.; Stang, P. J. *J. Am. Chem. Soc.* **2003**, *125*, 13950. (d) Kuehl, C. J.; Yamamoto, T.; Seidel, S. R.; Stang, P. J. *Org. Lett.* **2002**, *4*, 913.

(31) (a) Crowley, J. D.; Goshe, A. J.; Bosnich, B. *J. Chem. Soc., Chem. Commun.* **2003**, 2824. (b) Goshe, A. J.; Crowley, J. D.; Bosnich, B. *Helv. Chim. Acta* **2001**, *84*, 2971. (c) Goshe, A. J.; Bosnich, B. *Synlett* **2001**, 941.

(32) *Gold: Progress in Chemistry, Biochemistry, and Technology*; Schmidbaur, H., Ed.; Wiley: New York, 1999.

Chart 1



$\text{Ph}_2\text{P}(\text{CH}_2)_m\text{PPh}_2(\mu\text{-L}')_2(\text{OTf})_4$ .<sup>34</sup> In view of these findings, we envisioned that the molecular rectangle  $[\text{Au}_4(\mu\text{-PANP})_2(\mu\text{-bipy})_2](\text{OTf})_4$  ( $\mathbf{1}\cdot(\text{OTf})_4$ ) could be assembled from two  $\text{Au}_2(\mu\text{-PANP})^{2+}$  clips and two bipy (Scheme 1). Analogous to the cyclophanes containing 4,4'-bipyridinium groups<sup>35</sup> such as Stoddart's cyclobis(paraquat-*p*-phenylene) ion<sup>36</sup> (CBPQT<sup>4+</sup>), the gold rectangle is a receptor for the various aromatic molecules depicted in Chart 1. The complexation between  $\mathbf{1}^{4+}$  and the aromatic guests, which have different molecular dimensions, substituents, and extent of  $\pi$ -conjugation, provides insights into the factors which govern the stability of the host-guest complexes.

## Experimental Section

**General Method.** All of the syntheses were carried out in  $\text{N}_2$  atmosphere with standard Schlenck techniques. 9,10-Bis(diphenylphosphino)anthracene (PANP)<sup>12c</sup> and  $\text{Au}_2(\mu\text{-PANP})\text{Cl}_2$ <sup>29</sup> were synthesized according to the reported methods.  $\text{KAuCl}_4$  was purchased from Oxkem. Silver triflate,  $\text{Me}_2\text{S}$ , and 4,4'-bipyridine were purchased from Aldrich and used without being purified. All of the aromatic guests, obtained from Aldrich, were purified by recrystallization from hot ethanol. The solvents used were purified according to the literature procedures.<sup>37</sup> The software program Kaleidagraph version 3.5 was used to carry out

the nonlinear least-squares regression on the data of NMR and fluorescence titrations.

**Physical Methods.** UV-vis absorption and fluorescence spectra were recorded on a Hewlett-Packard HP8452A diode array spectrophotometer and a Perkin-Elmer LS50B spectrofluorophotometer, respectively. The averaged optical path length for the emitting light is 1 cm. Luminescence quantum yield was referenced to anthracene in chloroform ( $\Phi_{\text{std}} = 0.27$ ).<sup>38</sup>  $^1\text{H}$  and  $^{31}\text{P}\{^1\text{H}\}$  NMR spectra were recorded on a Bruker ACF 300 spectrometer. Elemental analyses were carried out in the department of chemistry, National University of Singapore. Electrospray ionization mass spectra (ESI-MS) were measured on a Finnigan MAT 731 LCQ spectrometer. Solid-state reflectance spectra were recorded on Shimadzu UV-2401 spectrophotometer equipped with a solid-state sample holder. The samples were prepared by grounding the crystals of the compounds in Nujol. Cyclic voltammetry was performed in a conventional two-compartment electrochemical cell with deaerated acetonitrile containing 0.1 M *n*-Bu<sub>4</sub>PF<sub>6</sub> as electrolyte. The glassy carbon disk working electrode (area 0.07 cm<sup>2</sup>) electrode was treated by polishing with 0.05  $\mu\text{m}$  alumina on a microcloth and then sonicated for 5 min in deionized water followed by rinsing with acetonitrile used in the electrochemical studies. An Ag/AgNO<sub>3</sub> (0.1 M in CH<sub>3</sub>CN) electrode was used as the reference electrode, whereas a platinum wire was used as the counter electrode. The half-wave potential ( $E_{1/2}$ ) values are the average of the cathodic and anodic peak potentials for the oxidative and reductive waves of reversible couples.<sup>39a</sup> The potential of the complex was always referred to the half-wave potential of the ferrocenium/ferrocene (Cp<sub>2</sub>Fe<sup>+0</sup>) couple as the internal reference.<sup>39b</sup>

**Determination of the Solubility of the Aromatic Guests.** The solubility of the aromatic guests was determined by the UV-vis absorption spectrometric method. Saturated solutions of the aromatic guests were then prepared by adding the large excess of the compounds to volumetric flasks containing 5 mL of CH<sub>3</sub>CN until solids appear. 1 mL of saturated solution was pipetted out and diluted to 50 mL or 100 mL. UV-vis absorption spectra of the diluted solutions were measured to give the absorbance of the  $\pi \rightarrow \pi^*$  bands. The concentrations of the compound in the saturated solutions were then determined from the extinction coefficients of the bands.

**Modified Job's Plot.** CD<sub>3</sub>CN solutions of  $[\text{G}]_t/([\text{G}]_t + [\text{H}]_t)$  ratio ranging from 0 to 1 were prepared ( $[\text{G}]_t$  and  $[\text{H}]_t$  are the total concentration of the guest and host, respectively). The sum of  $[\text{G}]_t$  and  $[\text{H}]_t$  was kept constant in all of the solutions. The stoichiometry of the host-guest complexation was determined from the *x*-coordinate at the maximum in a modified Job's plot in which the *y*-axis is  $[\text{G}]_t(\delta_G -$

- (33) (a) McArdle, C. P.; Van, S.; Jennings, M. C.; Puddephatt, R. J. *J. Am. Chem. Soc.* **2002**, *124*, 3959. (b) Hunks, W. J.; MacDonald, M.-A.; Jennings, M. C.; Puddephatt, R. J. *Organometallics* **2000**, *19*, 5063. (c) McArdle, C. P.; Irwin, M. J.; Jennings, M. C.; Puddephatt, R. J. *Angew. Chem., Int. Ed.* **1999**, *22*, 3376. (d) Qin, Z.; Jennings, M. C.; Puddephatt, R. J. *Chem.-Eur. J.* **2002**, *8*, 735. (e) McArdle, C. P.; Irwin, M. J.; Jennings, M. C.; Vittal, J. J.; Puddephatt, R. J. *Chem.-Eur. J.* **2002**, *8*, 723. (f) McArdle, C. P.; Vittal, J. J.; Puddephatt, R. J. *Angew. Chem., Int. Ed.* **2000**, *39*, 3819.
- (34) (a) Puddephatt, R. J. *J. Chem. Soc., Chem. Commun.* **1998**, 1055. (b) Irwin, M. J.; Vittal, J. J.; Yap, G. P. A.; Puddephatt, R. J. *J. Am. Chem. Soc.* **1996**, *118*, 13101. (c) Irwin, M. J.; Puddephatt, R. J.; Rendina, L. M.; Vittal, J. J. *J. Chem. Soc., Chem. Commun.* **1996**, 1281. (d) Brandys, M.-C.; Jennings, M. C.; Puddephatt, R. J. *J. Chem. Soc., Dalton Trans.* **2000**, 4601. (e) Burchell, T. J.; Eisler, D. J.; Jennings, M. C.; Puddephatt, R. J. *J. Chem. Soc., Chem. Commun.* **2003**, 2228.
- (35) Bühner, M.; Geuder, W.; Gries, W.-K.; Hüinig, S.; Koch, M.; Poll, T. *Angew. Chem., Int. Ed. Engl.* **1988**, *27*, 1553.
- (36) (a) Odell, B.; Reddington, M. V.; Slawin, A. M. Z.; Spencer, N.; Stoddart, J. F.; Williams, D. J. *Angew. Chem., Int. Ed. Engl.* **1988**, *27*, 1547. (b) Ashton, P. R.; Odell, B.; Reddington, M. V.; Slawin, A. M. Z.; Stoddart, J. F.; Williams, D. J. *Angew. Chem., Int. Ed. Engl.* **1988**, *27*, 1550. (c) Anelli, P. L.; Ashton, P. R.; Ballardini, R.; Balzani, V.; Delgado, M.; Gandolfi, M. T.; Goodnow, T. T.; Kaifer, A. E.; Philp, D.; Pietraszkiewicz, M.; Prodi, L.; Reddington, M. V.; Slawin, A. M. Z.; Spencer, N.; Stoddart, J. F.; Vicent, C.; Williams, D. J. *J. Am. Chem. Soc.* **1992**, *114*, 193. (d) Nielsen, M. B.; Jeppesen, J. O.; Lau, J.; Lomholt, C.; Damgaard, D.; Jacobsen, J. P.; Becher, J.; Stoddart, J. F. *J. Org. Chem.* **2001**, *66*, 3559.
- (37) Perrin, D. D.; Armarego, W. L. F. *Purification of Laboratory Chemicals*, 2nd ed.; Pergamon Press: Oxford, 1980.

(38) *CRC Handbook of Organic Photochemistry*; Scaiano, J. C., Ed.; CRC Press: Boca Raton, FL, 1989.

(39) (a) Gritzner, G.; Küta, J. *Pure Appl. Chem.* **1982**, *54*, 1527. (b) Gagné, R. R.; Koval, C. A.; Lisensky, G. C. *Inorg. Chem.* **1980**, *19*, 2855.

$\delta_G^o$ ) ( $\delta_G^o$  = chemical shifts of the free guest protons) and the  $x$ -axis is  $[G]_t/[G]_t + [H]_t$ .<sup>40a</sup>

**<sup>1</sup>H NMR Titrations.** In the <sup>1</sup>H NMR titrations,  $[G]_t$  is fixed while  $[H]_t$  is varied. The chemical shift  $\delta_G$  of certain protons of the guest is plotted against  $[H]_t$ . The binding constant  $K_{\text{NMR}}$ , and the chemical shift difference ( $\Delta\delta_G$ ) between the free guest ( $\delta_G^o$ ) and the complexed guest ( $\delta_G^c$ ), were obtained from nonlinear least-squares regression onto the data of the eq 1.<sup>40</sup>

$$\delta_G = \delta_G^o - \left( \frac{\Delta\delta_G}{2[G]_t} \right) (B - \sqrt{B^2 - 4[H]_t[G]_t}) \quad (1)$$

$$B = [H]_t + [G]_t + \frac{1}{K_{\text{NMR}}} \quad (1.1)$$

$\Delta\delta_H$  values for the host protons were also determined by similar least-squares fittings. In the cases of weakly binding guests, the shifts were very small and the  $\Delta\delta_H$  values were estimated as the largest chemical shifts observed in the titrations.

**Fluorescence Quenching Studies.** The emission spectra of CH<sub>3</sub>-CN solutions containing the same  $[H]_t$  but different  $[G]_t$  were recorded. The intensity ratio  $I_H/I_H^o$  ratio ( $I_H$  and  $I_H^o$  are the emission intensities of the host in the presence and absence of the guest, respectively) was plotted against  $[G]_t$ , and the binding constants  $K_Q$  were obtained by fitting by nonlinear least-squares regression with the eq 3 where  $k_{H-G}$  and  $k_H$  are constants related to the fluorescence intensities of the host-guest complex and host, respectively.<sup>41</sup>

$$\frac{I_H}{I_H^o} = 1 + \frac{\left( \frac{k_{H-G}}{k_H} \right) K_Q [G]_t}{1 + K_Q [G]_t} \quad (2)$$

In the quenching of the emission of the guests by the hosts, the emission spectra of solutions containing the same  $[G]_t$  but different  $[H]_t$  were recorded. The emission intensity of the guest ( $I_G$ ) at the wavelength  $\lambda$  of **1**·(OTf)<sub>4</sub> was measured. The data were best-fitted by a modified Beer's Law (eq 3),<sup>42</sup> where  $\epsilon$  is the extinction coefficient of the host at the wavelength  $\lambda$  and  $I_G^o$  is the emission intensity at  $[H]_t = 0$ .

$$\frac{I_G^o}{I_G} = \epsilon \times [H]_t \quad (3)$$

**X-ray Crystallography.** The diffraction experiments were carried out on a Bruker AXS SMART CCD 3-circle diffractometer with a sealed tube at 23 °C using graphite-monochromated Mo K $\alpha$  radiation ( $\lambda = 0.71073$  Å). The software used was as follows: SMART<sup>43a</sup> for collecting frames of data, indexing reflection, and determination of lattice parameters, SAINT<sup>43a</sup> for integration of intensity of reflections and scaling, SADABS<sup>43b</sup> for empirical absorption correction, and SHELXTL<sup>43c</sup> for space group determination, structure solution, and least-squares refinements on  $|F|^2$ . Anisotropic thermal parameters were refined for the rest of the non-hydrogen atoms. The hydrogen atoms were placed in their ideal positions. A brief summary of crystal data and experimental details are given in the Table S1, and the selected bond length, angles, and structural parameters are given in Tables 1 and 2.

## Results and Discussion

**Structure of Au<sub>2</sub>( $\mu$ -PANP)(NO<sub>3</sub>)<sub>2</sub>·0.5Et<sub>2</sub>O.** Complex Au<sub>2</sub>( $\mu$ -PANP)(NO<sub>3</sub>)<sub>2</sub> was synthesized from the reaction of Au<sub>2</sub>( $\mu$ -

**Table 1.** Selected Bond Lengths (Å) and Angles (deg) of Au<sub>2</sub>( $\mu$ -PANP)(NO<sub>3</sub>)<sub>2</sub>·0.5Et<sub>2</sub>O

|             |          |                   |          |
|-------------|----------|-------------------|----------|
| Au(1)–O(1B) | 2.11(2)  | P(1)–Au(1)–O(1A)  | 162.5(1) |
| Au(1)–O(1A) | 2.19(4)  | P(1)–Au(1)–O(2A)  | 145.0(8) |
| Au(1)–O(2A) | 2.43(3)  | P(1)–Au(1)–O(1B)  | 178.8(8) |
| Au(1)–P(1)  | 2.208(2) | O(1A)–Au(1)–O(1B) | 49.6(6)  |
| Au(2)–O(4)  | 2.092(7) | P(2)–Au(2)–O(4)   | 177.0(3) |
| Au(2)–P(2)  | 2.213(2) |                   |          |
| Au(1)–Au(2) | 3.375(6) |                   |          |

PANP)Cl<sub>2</sub> and 2 mol equiv of AgNO<sub>3</sub> in CH<sub>2</sub>Cl<sub>2</sub>. The X-ray crystal structure of the complex (Figure 1 and Table 1) shows a U-shape geometry similar to that of Au<sub>2</sub>( $\mu$ -PANP)Cl<sub>2</sub>.<sup>29</sup> The two gold atoms Au(1) and Au(2) are syn to each other and separated by 9.197(3) Å. Au(2) is coordinated linearly to an O atom of the NO<sub>3</sub><sup>−</sup> ion and a P atom of the PANP (P(2)–Au(2)–O(4) = 177.0(3)°). On the other hand, the NO<sub>3</sub><sup>−</sup> ion bonded to Au(1) is disordered. The Au–P distances are typical,<sup>29,44</sup> and the Au(2)–O(4) (2.092(7) Å) and Au(1)–O(1B) (2.11(2) Å) distances are close to the ones observed in Au(PMe<sub>3</sub>)(NO<sub>3</sub>) (Au–O = 2.093(6) Å).<sup>44</sup> The central anthracenyl backbone is slightly curve toward the metal ions, and the dihedral angle between the two lateral rings is 15.5°. In the crystal, the molecules aggregate into dimers, showing an intermolecular Au–Au distance of 3.375(3) Å. Similar Au–Au distances (~2.9–3.5 Å), observed widely in the solid-state aggregations of Au<sup>I</sup> complexes, have been taken as the structural evidence for aurophilic interactions.<sup>45</sup> In addition, the two concaved anthracenyl rings partially overlap, and the separation between their best planes is 3.7 Å, which is typical for aromatic  $\pi$ – $\pi$  interactions.<sup>46</sup> It is possible that the solid-state aggregation of the gold complex is the result of cooperative actions of aurophilic and aromatic  $\pi$ – $\pi$  interactions. The <sup>31</sup>P NMR spectrum (121.5 MHz, CDCl<sub>3</sub>) of the complex shows a singlet at  $\delta$  20.31. This indicates that complex reverts to C<sub>2v</sub> symmetry in solution with both NO<sub>3</sub><sup>−</sup> ions adopting the same coordination mode.

**Synthesis of the Gold Rectangle.** The gold rectangle [Au<sub>4</sub>( $\mu$ -PANP)<sub>2</sub>( $\mu$ -bipy)<sub>2</sub>](NO<sub>3</sub>)<sub>4</sub> (**1**·(NO<sub>3</sub>)<sub>4</sub>) was synthesized in a high yield of 82% by reacting the molecular “clip” Au<sub>2</sub>( $\mu$ -PANP)(NO<sub>3</sub>)<sub>2</sub> with 1 mol equiv of 4,4′-bipyridine (bipy) in CH<sub>2</sub>Cl<sub>2</sub> for 5 h (Scheme 1). The product **1**·(NO<sub>3</sub>)<sub>4</sub> was slowly precipitated from the reacting solution as yellow solids. Metatheses of **1**·(NO<sub>3</sub>)<sub>4</sub> with NaOTf, LiClO<sub>4</sub>, and NaPF<sub>6</sub> gives **1**·(OTf)<sub>4</sub>, **1**·(ClO<sub>4</sub>)<sub>4</sub>, and **1**·(PF<sub>6</sub>)<sub>4</sub>, respectively. While **1**·(NO<sub>3</sub>)<sub>4</sub> is entirely insoluble in CH<sub>2</sub>Cl<sub>2</sub>, CH<sub>3</sub>CN, and MeOH but dissolves fairly well in a mixture of CH<sub>2</sub>Cl<sub>2</sub>/MeOH (8:2, v/v), the other three compounds are soluble in CH<sub>3</sub>CN and a CH<sub>2</sub>Cl<sub>2</sub>/MeOH mixture but sparingly soluble in CH<sub>2</sub>Cl<sub>2</sub>. The <sup>1</sup>H NMR spectra of all of the gold complexes are basically identical and will be discussed later. Consistent with the rectangular structure of **1**<sup>4+</sup>, the <sup>31</sup>P-<sup>1</sup>H NMR spectra of the four complexes display a singlet at similar chemical shift ( $\delta$  21.35–22.89).

The ESI-MS spectra of **1**·(NO<sub>3</sub>)<sub>4</sub>, **1**·(OTf)<sub>4</sub>, **1**·(ClO<sub>4</sub>)<sub>4</sub>, and **1**·(PF<sub>6</sub>)<sub>4</sub> (Figures S1–S20) measured in CH<sub>3</sub>CN display sig-

(40) (a) Hirose, K. *J. Inclusion Phenom. Macrocyclic Chem.* **2001**, *39*, 193. (b) Macomber, R. S. *J. Chem. Educ.* **1992**, *69*, 375.

(41) Connors, K. A. *Binding Constants: The Measurement of Molecular Complex Stability*; Wiley-Interscience: New York, 1987; pp 24–28.

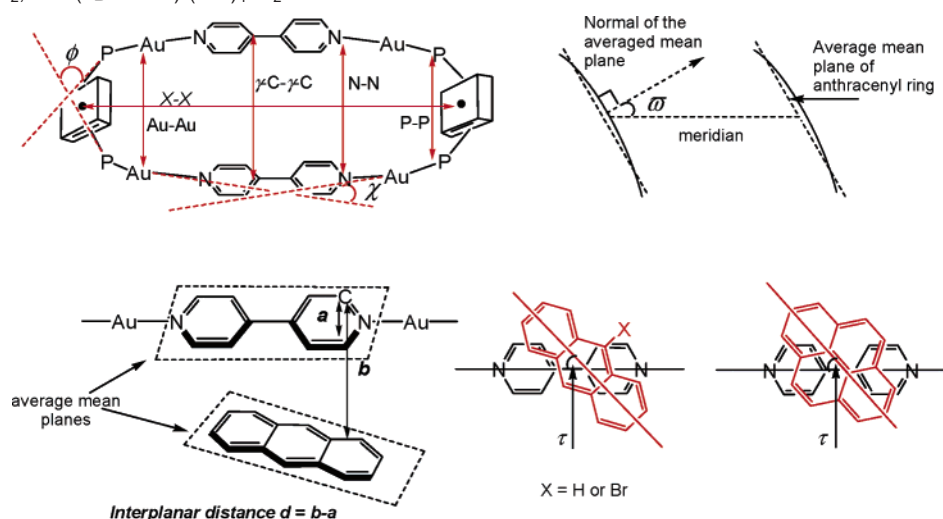
(42) *Physical Chemistry: Principles and Applications in Biological Sciences*; Tinoco, I., Jr., Sauer, K., Wang, J. C., Eds.; Prentice Hall: New Jersey, 1995; pp 388–390.

(43) (a) *SMART & SAINT Software Reference Manuals*, Version 4.0; Siemens Energy & Automation, Inc., Analytical Instrumentation: Madison, WI, 1996. (b) Sheldrick, G. M. *SADABS: a Software for Empirical Absorption Correction*; University of Gottingen: Gottingen, Germany, 1996. (c) *SHELXTL Reference Manual*, Version 5.03; Siemens Energy & Automation, Inc., Analytical Instrumentation: Madison, WI, 1996.

(44) Mathieson, T.; Schier, A.; Schmidbaur, H. *J. Chem. Soc., Dalton Trans.* **2000**, 3881.

(45) (a) Schmidbaur, H. *Gold Bull.* **1990**, *23*, 11. (b) Schmidbaur, H. *Chem. Soc. Rev.* **1995**, *24*, 391.

(46) Hunter, C. A.; Sanders, J. K. M. *J. Am. Chem. Soc.* **1990**, *112*, 5525.

**Table 2.** Selected Bond Length (Å), Angles (deg), and Other Structural Parameters of **1** (OTf)<sub>4</sub>·4.8H<sub>2</sub>O, (1▷An)·(OTf)<sub>4</sub>, (1▷Py)·(OTf)<sub>4</sub>·CH<sub>2</sub>Cl<sub>2</sub>, and (1▷Br-An)·(OTf)<sub>4</sub>·Et<sub>2</sub>O

|                          | <b>1</b> (OTf) <sub>4</sub> ·4.8H <sub>2</sub> O | (1▷An)·(OTf) <sub>4</sub> | (1▷Py)·(OTf) <sub>4</sub> ·CH <sub>2</sub> Cl <sub>2</sub> | (1▷Br-An)·(OTf) <sub>4</sub> ·Et <sub>2</sub> O |
|--------------------------|--|---------------------------|--|---|
| Au–Au <sup>a</sup> (Å)   | 7.069(3)   | 6.854(2)                  | 6.811(2)   | 6.526(2), 6.604(2)                              |
| P–P <sup>a</sup> (Å)     | 6.375(3)   | 6.351(3)                  | 6.342(2)   | 6.255(4), 6.256(4)                              |
| N–N <sup>a</sup> (Å)     | 7.665(3)   | 7.229(2)                  | 7.102(3)   | 6.767(4), 6.910(4)                              |
| γ-C–γ-C <sup>a</sup> (Å) | 7.921(3)   | 7.341(4)                  | 7.187(3)   | 6.980(4), 6.981(4)                              |
| Au(1)–P(1) (Å)           | 2.255(2)   | 2.239(3)                  | 2.247(4)   | 2.240(4), 2.246(4)                              |
| Au(1)–N(1) (Å)           | 2.044(1)   | 2.052(3)                  | 2.063(1)   | 2.073(1), 2.071(1)                              |
| C(6)–P(1)–Au(1) (deg)    | 108.7(3)   | 110.0(3)                  | 110.4(1)   | 109.4(5), 109.5(5)                              |
| P(1)–Au(1)–N(1) (deg)    | 177.4(4)   | 178.5(3)                  | 177.7(3)   | 175.0(4), 178.5(5)                              |
| Au(1)–N(1)–C(3) (deg)    | 173.4(4)   | 175.9(4)                  | 176.8(3)   | 175.6(4), 176.4(4)                              |
| N(1)–C(3)–C(3a) (deg)    | 175.8(3)   | 177.5(3)                  | 178.7(2)   | 177.5(4)  |
| d <sup>b</sup> (Å)       |  | 3.645(2)                  | 3.552(8)   | 3.401(4)  |
| X–X <sup>c</sup> (Å)     | 16.76  | 16.76                     | 17.05  | 16.95   |
| θ <sup>d</sup> (deg)     | 21.69  | 10.42                     | 3.60   | 2.71  |
| ω <sup>e</sup> (deg)     | 43.7   | 43.3                      | 47.4   | 56.5, 49.9                                      |
| φ <sup>f</sup> (deg)     | 22.3   | 30.5                      | 31.4   | 40.0  |
| χ <sup>g</sup> (deg)     | 16.8   | 10.5                      | 8.0  | 13.2  |
| τ <sup>h</sup> (deg)     |  | 12.4                      | 0.9  | 25.9  |
| ε <sup>i</sup> (deg)     | 16.4   | 14.7                      | 21.9   | 21.4, 19.4                                      |

<sup>a</sup> Intramolecular Au–Au, P–P, N–N, and γ-C–γ-C distances. <sup>b</sup> *d* = interplanar distance between the 4,4'-bipyridine and the aromatic guest, defined as the difference between *b* (the perpendicular distance between a carbon atom and the plane of the aromatic guest) and *a* (distance between the carbon atom in the best plane of bipy). <sup>c</sup> X–X = distance between the centroids of the two anthracenyl rings in **1**<sup>4+</sup>. <sup>d</sup> θ = twist angle between the two pyridyl rings of the bipy. <sup>e</sup> ω = tilt angle of the anthracenyl rings, defined as the angle between the normal of the best plane of the anthracenyl ring and the long meridian of the rectangle. <sup>f</sup> φ = angle subtended by the two P–C bonds of the PAnP ligand. <sup>g</sup> χ = angle subtended by the two Au–N bonds. <sup>h</sup> τ = angle between the long axis of the aromatic guest and the central axis of the bipy. <sup>i</sup> ε = dihedral angle between the lateral rings in the anthracenyl ring.

nificant peaks which can be attributed to the triply charged species (**1**<sup>4+</sup>+NO<sub>3</sub>)<sup>3+</sup> (*m/z* 751.39, calcd. 751.77), (**1**<sup>4+</sup>+OTf)<sup>3+</sup> (*m/z* 780.37, calcd. 780.76), (**1**<sup>4+</sup>+ClO<sub>4</sub>)<sup>3+</sup> (*m/z* 763.51 calcd. 764.09), and (**1**<sup>4+</sup>+PF<sub>6</sub>)<sup>3+</sup> (*m/z* 779.18, calcd. 779.43), respectively. The assignments are further confirmed by calculated isotopic distributions. The most prominent peaks in the spectra of **1**·(NO<sub>3</sub>)<sub>4</sub>, **1**·(OTf)<sub>4</sub>, and **1**·(ClO<sub>4</sub>)<sub>4</sub> belong to the “half-rectangle” [Au<sub>2</sub>(μ-PAnP)(bipy)+X]<sup>+</sup> (X = NO<sub>3</sub><sup>−</sup>, OTf<sup>−</sup>, and ClO<sub>4</sub><sup>−</sup>). On the other hand, no “half-rectangle” peak is observed in the ES-MS of **1**·(PF<sub>6</sub>)<sub>4</sub>. Instead, the largest peak of the spectrum at *m/z* 1241.40 (calcd. 1241.6) is identified by simulated isotopic distributions as doubly charged (**1**<sup>4+</sup>+2PF<sub>6</sub>)<sup>2+</sup> (Figures S17, 18). These results lend support to the rectangular structure of **1**<sup>4+</sup> and suggest the stability of the gold complexes in solutions. Elemental analyses of the compounds also agree well with the proposed molecular formulas. The structure of **1**·(OTf)<sub>4</sub> was confirmed by X-ray crystallography (vide infra). Among all of these salts, **1**·(OTf)<sub>4</sub> is the only one that can be crystallized, and hence is the focus of the present study.

A simpler and nearly quantitative synthesis (yield = 90%) of **1**·(OTf)<sub>4</sub> involves the reaction of Au<sub>2</sub>(μ-PAnP)(OTf)<sub>2</sub> generated in situ from the reaction of (AuCl)<sub>2</sub>(μ-PAnP) and AgOTf in CH<sub>2</sub>Cl<sub>2</sub>, with 1 mol equiv of bipy. Attempts to isolate Au<sub>2</sub>(μ-PAnP)(OTf)<sub>2</sub> were unsuccessful as the compound slowly decomposes in the solid state. Nonetheless, the <sup>31</sup>P NMR spectrum (121.5 MHz, CD<sub>2</sub>Cl<sub>2</sub>) of Au<sub>2</sub>(μ-PAnP)(OTf)<sub>2</sub> prepared in situ shows a singlet at δ 21.66, suggesting that the complex could have a C<sub>2v</sub> “clip”-like structure similar to that of Au<sub>2</sub>(μ-PAnP)(NO<sub>3</sub>)<sub>2</sub>. The self-assembly of **1**·(OTf)<sub>4</sub> is completed within 5 h at room temperature, as indicated by the precipitation of the product from the solution.

That the reaction between the digold(I) clip and bipy gives the molecular rectangle as the major product suggests that the macrocyclic **1**<sup>4+</sup> ion is either thermodynamically or kinetically stable. Apparently, entropy would favor the formation of discrete rectangle over polymer. An additional driving force for the formation of the gold rectangle could come from the insolubility of the metallacyclophane in reacting solvent CH<sub>2</sub>Cl<sub>2</sub>, as the

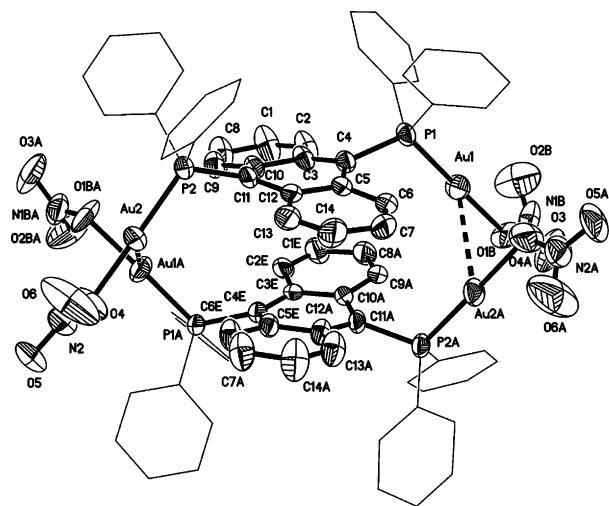


**Figure 1.** ORTEP diagram of  $\text{Au}_2(\mu\text{-PANP})(\text{NO}_3)_2 \cdot 0.5\text{Et}_2\text{O}$  showing the dimerization of the complex in the solid state via aurophilic attraction. Hydrogen atoms and solvent molecules are omitted for clarity. Thermal ellipsoids are shown at 50% probability.

precipitation would shift the equilibrium toward the formation of the metallacyclophane. The syn-orientation of the two Au atoms in the molecular clips  $\text{Au}_2(\mu\text{-PANP})(\text{X})_2$  ( $\text{X} = \text{NO}_3^-$  and  $\text{OTf}^-$ ) would also favor the formation of the macrocyclic structure, as in the case of the metallacycle  $[\text{Au}_4(\mu\text{-Ph}_2\text{PCH}_2\text{-PPh}_2)_2(\mu\text{-bipy})_2](\text{CF}_3\text{CO}_2)_4$ .<sup>34a-d</sup> As will be discussed later, it appears that the macrocyclic  $\mathbf{1}^{4+}$  is also stabilized kinetically: once formed, the complex would be locked in the rectangular structure and would not open up to form the polymer.

The self-assembly is sensitive to the anions: when  $\text{AgClO}_4$  or  $\text{AgBF}_4$  is used instead of  $\text{AgCF}_3\text{SO}_3$ , the reported ring-like compound  $[\text{Au}_3(\mu\text{-PANP})_3\text{OClO}_4](\text{ClO}_4)_2$ <sup>12e</sup> or  $[\text{Au}_3(\mu\text{-PANP})_3\text{OBF}_4](\text{BF}_4)_2$ <sup>47</sup> is identified by NMR and X-ray crystallography as the major product. It is possible that the tetrahedral  $\text{ClO}_4^-$  and  $\text{BF}_4^-$  ions have a template effect that promotes the ring formation. In fact, like many other metallacycles arising from anion-templation,<sup>2d,10a,19a,48</sup> the gold rings encapsulate an anion in their cavities.  $\mathbf{1} \cdot (\text{OTf})_4$  is infinitely stable in the solid state but undergoes slow decomposition in solution under light.

**X-ray Crystal Structure of  $\mathbf{1} \cdot (\text{OTf})_4 \cdot 4.8\text{H}_2\text{O}$ .** The crystals of  $\mathbf{1} \cdot (\text{OTf})_4 \cdot 4.8\text{H}_2\text{O}$  were obtained from slow diffusion of ether into a  $\text{CH}_2\text{Cl}_2/\text{MeOH}$  (8:2, v/v) solution of the gold compound. The X-ray crystal structure  $\mathbf{1} \cdot (\text{OTf})_4 \cdot 4.8\text{H}_2\text{O}$  reveals a tetracation  $\mathbf{1}^{4+}$  comprising two opposite  $[\text{Au}_2(\mu\text{-PANP})]^{2+}$  units linked by two bipy ligands (Figure 2 and Table 2, see scheme for Table 2 for the definitions of the structural parameters). The  $\mathbf{1}^{4+}$  ion has a rectangular shape and is fenced on its four sides by the anthracenyl and pyridyl rings. The  $\mathbf{1}^{4+}$  ion shows an approximate  $C_{2h}$  symmetry where the  $C_2$  axis bisects the two pyridyl rings of the bipy and the center of inversion coincides with the center of the rectangle. Four disordered  $\text{OTf}^-$  ions are located around the rim of each  $\mathbf{1}^{4+}$  ion. In the center of the molecule is a large cavity (Figure 2a). The length of the rectangle, taken as the

distance between the centroids of the opposite anthracenyl rings X–X, is 16.76(3) Å, and its width, taken as the distance between the  $\gamma$ -carbon atoms ( $\gamma\text{-C}-\gamma\text{-C}$ ) of the two opposite bipy, is 7.921(3) Å. The cavity of  $\mathbf{1}^{4+}$  is significantly larger than that of  $\text{CBPQT}^{4+}$  ion, which is also rectangular in shape ( $6.8 \times 10.3$  Å).<sup>36a</sup>

The  $\mathbf{1}^{4+}$  ion is slightly bellied on its four sides. For the two sides of the rectangle, the angle  $\chi$  subtended by the two Au–N bonds is 16.8°. The bulging is due to the C(anthracenyl)–P(1)–Au(1) angle (108.7(3)°), the bending of the bipy (N(1)–C(3)–C(3A) = 175.8(3)°), and the small offset between the central axis of the bipy and the Au–P bond (Au(1)–N(1)–C(3) = 173.4(4)°). The out-of-plane distortion of the central ring of the anthracenyl backbone, indicated by the angle  $\phi$  of 22.3° subtended by the P–C(anthracenyl) bonds, is responsible for the bulging at the two ends of the rectangle. The distortion significantly shortens the Au–Au distance to 7.069(3) Å (cf. 9.154(2) Å in  $\text{Au}_2(\mu\text{-PANP})(\text{NO}_3)_2$ ). The anthracenyl rings are curved away from the Au atoms, and the dihedral  $\epsilon$  between the two lateral rings of the anthracenyl backbone is 16.4°. Apparently, the shortening of the Au–Au distance is to maintain the linear metal coordination (P(1)–Au(1)–N(1) = 177.4(4)°), which is known to be the preferential geometry of  $\text{Au}^{\text{I}}$  ion. The two pyridyl rings of the bipy are not coplanar, showing a twist angle  $\theta$  of 21.69°. The Au–P and Au–N bond lengths are normal. The two opposite anthracenyl rings are parallel and tilted toward one end of the rectangle. The tilt angle  $\omega$ , defined as the angle between the normal of the ring and long meridian X–X of the rectangle, is 43.7°. The eight phenyl rings in  $\mathbf{1}^{4+}$  can be grouped into two geometrically different sets: four axially oriented phenyl rings ( $\text{Ph}_{\text{ax}}$ ) and four equatorially oriented phenyl rings ( $\text{Ph}_{\text{eq}}$ ) (Figure 2b). Possibly, the anthracenyl rings are tilted to minimize the steric repulsion with the  $\text{Ph}_{\text{ax}}$  rings. The  $\text{Ph}_{\text{ax}}$  rings at the two ends of  $\mathbf{1}^{4+}$  are pointing to opposite directions and are related by a  $C_2$  rotation. Similarly, the four  $\text{Ph}_{\text{eq}}$  rings are equivalent. However, the  $\text{Ph}_{\text{ax}}$  rings are diastereotopic with the  $\text{Ph}_{\text{eq}}$  rings.

**Solution Structure of  $\mathbf{1} \cdot (\text{OTf})_4$ .** Some metallacyclophanes are known to dissociate or undergo dynamic exchanges with other oligomeric or polymeric structures in solutions.<sup>7b,8h,s</sup> Of particular relevance to the present study is the work of the Puddephatt group which suggested the presence of equilibria between tetragold(I) metallacycles  $[\text{Au}_4(\mu\text{-PPh}_2(\text{CH}_2)_m\text{PPh}_2)_2(\mu\text{-L}')_2](\text{CF}_3\text{CO}_2)_4$  ( $m = 3-6$ ,  $\text{L}' = \text{bipy}$ ,  $\text{bpe}$ , or 1,4-diisocyanobenzene) and coordination polymers  $[\text{Au}_2(\mu\text{-PPh}_2(\text{CH}_2)_m\text{-PPh}_2)(\mu\text{-L}')_n](\text{CF}_3\text{CO}_2)_{2n}$ ,<sup>34</sup> and other species arising from the ring opening.<sup>34c</sup> However, it is believed that the gold rectangle is stable and retains its macrocyclic structures in solution. First of all, if  $\mathbf{1} \cdot (\text{OTf})_4$  equilibrates with the polymer  $[\text{Au}_2(\mu\text{-PANP})(\mu\text{-bipy})_n](\text{OTf})_n$ , or other oligomeric species in solution, one would expect significant broadening  $^1\text{H}$  and  $^{31}\text{P}$  NMR signals and even the appearance of new peaks at low temperature. However, the  $^{31}\text{P}\{^1\text{H}\}$  NMR spectrum ( $\text{CD}_3\text{CN}$ , 121 MHz) (Figure S21) of the complex displays a singlet at  $\delta$  22.76 whose line shape remains unchanged even at 243 K. On the other hand, the  $^1\text{H}$  NMR signals are slightly broadened as the temperature is lowered from 298 to 243 K (Figure S21). Nonetheless, it can be aptly explained by a fluxional process involving the flipping of the anthracenyl rings (Scheme 2): In contrast to the X-ray crystal structure of  $\mathbf{1}^{4+}$  in which the two ends of the tilted

(47) Prabhavathy, J. M. Sc. Thesis, National University of Singapore.

(48) (a) Mann, S.; Huttner, G.; Zsolnai, L.; Heinze, K. *Angew. Chem., Int. Ed. Engl.* **1996**, *35*, 2808. (b) Hasenkopf, B.; Lehn, J.-M.; Boumediene, N.; Dupont-Gervais, A.; Van Dorsselaer, A.; Kniessel, B.; Fenske, D. *J. Am. Chem. Soc.* **1997**, *119*, 10956. (c) Fleming, J. S.; Mann, K. L. V.; Carraz, C.-A.; Psillakis, E.; Jeffrey, J. C.; McCleverty, J. A.; Ward, M. D. *Angew. Chem., Int. Ed.* **1998**, *37*, 1279. (d) Schnebeck, R.-D.; Freisinger, E.; Lippert, B. *Angew. Chem., Int. Ed.* **1999**, *38*, 168.



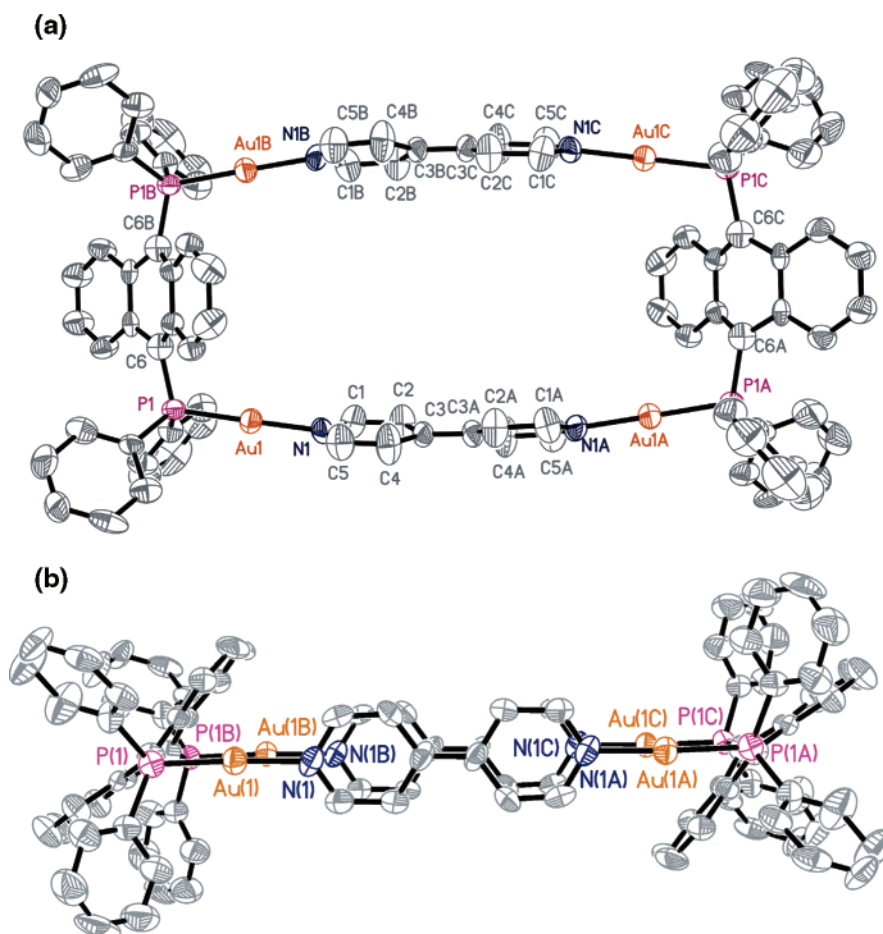
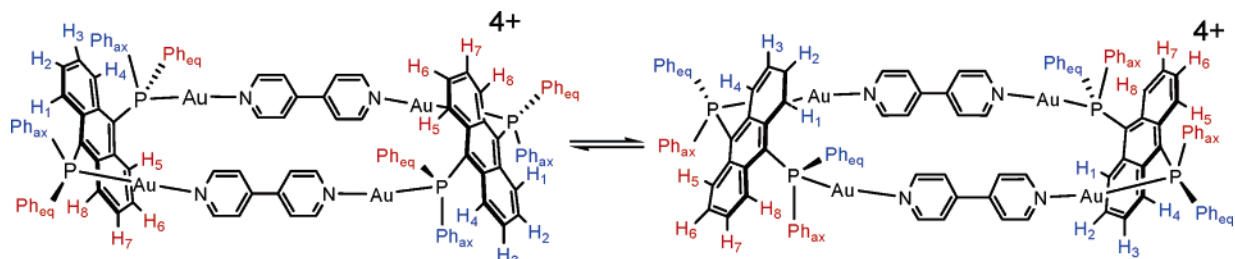


**Figure 2.** ORTEP diagrams of  $1^+(OTf)_4 \cdot 4.8H_2O$  showing (a) the top view and (b) the side view of the  $1^{4+}$  ion. (b) Hydrogen atoms, anions, and  $H_2O$  molecules are omitted for clarity. Thermal ellipsoids are shown at 50% probability.

**Scheme 2.** Proposed Anthracenyl Ring Flipping of  $1^{4+}$



anthracenyl rings are nonequivalent (i.e.,  $H_{2,3} \neq H_{6,7}$ ,  $H_{1,4} \neq H_{5,8}$ ), the room-temperature  $^1H$  NMR spectrum of the complex shows two multiplets at  $\delta$  7.34 and 8.42 attributable to  $H_{1,4,5,8}$  and  $H_{2,3,6,7}$ , respectively. The merge of signals signifies a fast exchange between  $H_{2,3} \rightleftharpoons H_{6,7}$  and  $H_{1,4} \rightleftharpoons H_{5,8}$  in solution. The exchange involves flipping of the anthracenyl rings which occurs concomitantly with a swapping between the diastereotopic  $Ph_{ax}$  and  $Ph_{eq}$  ( $Ph_{ax} \rightleftharpoons Ph_{eq}$ ). Because the two exchanging partners are identical, the P atoms should remain equivalent throughout the process. In accord with this is the invariable singlet observed in the VT  $^31P\{^1H\}$  NMR measurements.

Another piece of evidence supporting the integrity of the  $1^{4+}$  ion in solution comes from our binding studies. As will be mentioned later,  $^1H$  NMR and fluorescence titrations unambiguously show that  $1^{4+}$  forms 1:1 complexes with various aromatic molecules (Chart 1). The binding of all of the guests to  $1^{4+}$  can be properly described by an equilibrium which involves only

three species:  $1^{4+}$  (host), the aromatic guests, and the host-guest complex. This indicates that  $1^{4+}$  does not dissociate or is not in equilibrium with other species in solution. The similar NMR spectroscopic properties displayed by  $1^+(NO_3)_4$ ,  $1^+(ClO_4)_4$ , and  $1^+(PF_6)_4$  also indicate that the rectangular structure of  $1^{4+}$  is not affected by its counterion.

The fact that  $1^{4+}$  retains its macrocyclic structure in solution could be due to kinetic stabilization. Recently, Stang et al. have demonstrated that the molecular rectangles  $[Pt_4(PEt_3)_8(\mu\text{-anth}^{2-})_2(\mu\text{-L})_2](X)_4$  ( $L = \text{bipy, bpe, 1,4-bis(4-ethynylpyridyl)benzene, 2,5-bis(4-ethynylpyridyl)furan, X = ClO}_4^-, PF_6^-, BF_4^-)$  are kinetically stable with respect to dissociation as the weakly nucleophilic anions are unable to displace the didipyridyl ligands.<sup>9g</sup> Similarly, the  $OTf^-$ ,  $ClO_4^-$ , and  $PF_6^-$  ions in the gold complexes, being poor electron donors, should not be able to substitute the bipy in  $1^{4+}$ . Furthermore, the anthracenyl rings, oriented almost perpendicular to the plane of the rectangle,

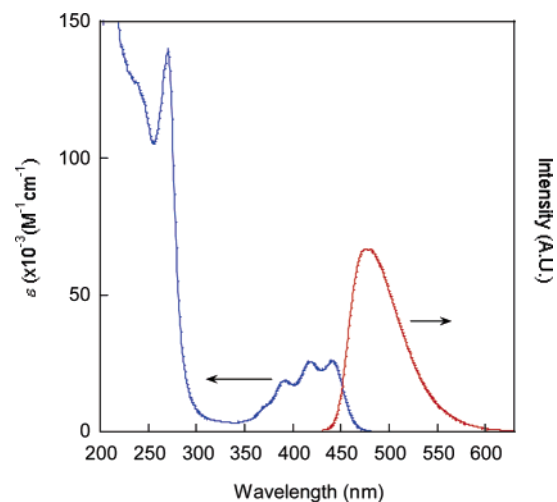


**Figure 3.** UV-vis absorption (blue) and emission (red) spectra of  $\mathbf{1}\cdot(\text{OTf})_4$ . Solvent:  $\text{CH}_3\text{CN}$ ,  $T = 298\text{ K}$ . Excitation wavelength = 420 nm, excitation and emission slit widths = 10 nm.

would possibly shield the gold atoms from the attack of the anion. These could be the reasons for the exceptional stability of  $\mathbf{1}^{4+}$  in comparison to other gold metallacycles.

**UV-Vis Absorption and Luminescence of  $\mathbf{1}\cdot(\text{OTf})_4$ .** The UV-vis absorption spectrum (Figure 3) of  $\mathbf{1}\cdot(\text{OTf})_4$  displays a very intense band at 270 nm ( $\epsilon_{\text{max}} = 1.4 \times 10^5\text{ M}^{-1}\text{ cm}^{-1}$ ), which corresponds to the high-energy  $^1\pi \rightarrow \pi^*$  transition of the anthracenyl rings. In addition, there is a moderately intense absorption band in 320–480 nm which displays vibronic peaks at 367, 390, 418, and 441 nm ( $\lambda_{\text{max}} = 441\text{ nm}$ ,  $\epsilon_{\text{max}} = 2.6 \times 10^4\text{ M}^{-1}\text{ cm}^{-1}$ ). The absorption band arises from the low energy  $^1\pi \rightarrow \pi^*$  transition of the anthracenyl ring. Similar absorption bands are found in the spectra of other PANP-containing complexes such as  $[\text{Au}_3(\mu\text{-PANP})_3\text{ClO}_4](\text{ClO}_4)_2$ .<sup>12c</sup> Irradiating an aerated  $\text{CH}_3\text{CN}$  solution of  $\mathbf{1}\cdot(\text{OTf})_4$  at 420 nm gives an emission maximized at 480 nm with quantum yield of 0.05 (Figure 3). The small Stoke shift indicates that the emission is  $^1\pi^* \rightarrow \pi$  fluorescence.  $[\text{Au}_3(\mu\text{-PANP})_3\text{ClO}_4](\text{ClO}_4)_2$  displays emission of similar energy and band shape.<sup>12c</sup>

**Electrochemistry of  $\mathbf{1}\cdot(\text{OTf})_4$ .** The room-temperature cyclic voltammogram (CV) of a  $\text{CH}_3\text{CN}$  solution of  $\mathbf{1}\cdot(\text{OTf})_4$  is shown in Figure 4. Upon reduction, an irreversible peak (a) appears at about  $-1.2\text{ V}$  versus  $\text{Cp}_2\text{Fe}^{+/0}$ . This is followed by a small quasi-reversible couple (b,b') at  $E_{1/2}$  of  $-1.38\text{ V}$  ( $\Delta E_i \approx 80\text{ mV}$ ). The irreversible peak (a) is likely a metal-centered reduction as most  $\text{Au}^{\text{I}}$ -phosphine compounds show a metal-centered irreversible reduction at similar potential in acetonitrile.<sup>49</sup> Holding the potential of the working electrode at  $-1.2\text{ V}$  also leads to slow deposition of gold metal on the electrode surface which can be observed with the naked eye. The reversible couple (b,b') is attributed to redox reaction centered at the bipy in  $\mathbf{1}^{4+}$  by comparison with the voltammogram of the Pt-rectangle  $[\text{Pt}_4(\text{PEt}_3)_8(\mu\text{-anth}^{2-})_2(\mu\text{-bipy})_2]^{4+}$  (which has the same charge as  $\mathbf{1}^{4+}$  and also shows a bipy-centered reduction at  $-1.44\text{ V}$ ).<sup>50</sup> The irreversible nature of wave (a) indicates that  $\mathbf{1}^{4+}$  decomposes upon reduction. Further scanning the potential toward the cathodic side leads to the appearance of two small reversible couples (c,c') and (d,d') at  $E_{1/2}$  of  $-1.9\text{ V}$  ( $\Delta E_i = 70$

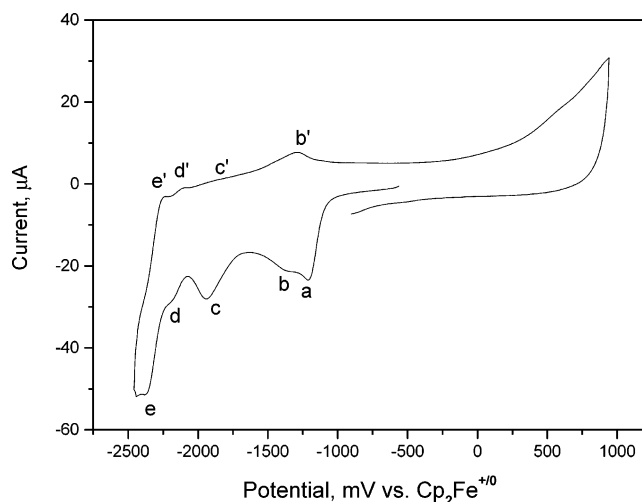


**Figure 4.** Cyclic voltammogram of  $\mathbf{1}\cdot(\text{OTf})_4$ . Solvent,  $\text{CH}_3\text{CN}$  (0.1 M  $n\text{-Bu}_4\text{NPF}_6$ ); working electrode, glassy carbon; counter electrode, platinum wire; reference electrode,  $\text{Ag}/\text{AgNO}_3$  (0.1 M in  $\text{CH}_3\text{CN}$ ).

mV) and  $-2.2\text{ V}$  ( $\Delta E_i = 70\text{ mV}$ ), respectively. As the CV (Figures S22) of the free PANP ligand also shows two similar reversible couples at  $-1.9$  and  $-2.2\text{ V}$ , these two couples can be assigned to the reduction of PANP liberated from  $\mathbf{1}^{4+}$  after decomposition. However, it is noted that the cathodic wave (c) in the voltammogram of  $\mathbf{1}^{4+}$  is much larger than its anodic counterpart (c'). A differential pulse voltammetric study on wave (c) shows that it is actually an overlap of two waves. Scanning the potential of the working electrode to  $-1.9\text{ V}$  also leads to deposition of gold metal on the electrode surface. We thus attribute wave (c) to be an overlap of two reduction processes, the reversible reduction of free PANP and the irreversible reduction of  $\text{Au}^{\text{I}}$  species generated from the decomposition of  $\mathbf{1}^{4+}$  as a result of reduction wave (a). The appearance of more than one  $\text{Au}^{\text{I}}$  reduction wave is commonly observed in polynuclear  $\text{Au}^{\text{I}}$  clusters.<sup>49</sup> The couple (e,e') at  $E_{1/2}$  of  $-2.3\text{ V}$  is due to the bipy generated from the cathodic decomposition of  $\mathbf{1}^{4+}$ , as the free ligand also shows a reversible couple at the same potential (Figure S23). A small irreversible wave attributable to the oxidation of decomposed product from  $\mathbf{1}^{4+}$  appears in the reverse anodic scan. No oxidation wave is observed if the initial voltammetric scan is made toward the anodic side.

The electrochemistry of  $\mathbf{1}\cdot(\text{OTf})_4$  is drastically different from that reported for the CBPQT<sup>4+</sup>, and the bipy-containing rectangles  $[\text{Pt}_4(\text{PEt}_3)_8(\mu\text{-anth}^{2-})_2(\mu\text{-bipy})_2](\text{PF}_6)_4$ <sup>50</sup> and  $[\text{Re}_4(\text{CO})_{12}(\mu\text{-bipy})(\text{bipm})_2]$ ,<sup>51</sup> which are dominated by ligand-centered redox processes. The organic cyclophane CBPQT<sup>4+</sup> exhibits two quasi-reversible two-electron couples at  $E_{1/2} = 0.59\text{ V}$  and  $-1.01\text{ V}$  (vs  $\text{Cp}_2\text{Fe}^{+/0}$ ) which correspond to bipyridinium-centered two-electron reductions. Similarly, the CV of  $[\text{Pt}_4(\text{PEt}_3)_8(\mu\text{-anth}^{2-})_2(\mu\text{-bipy})_2](\text{PF}_6)_4$  and  $[\text{Re}_4(\text{CO})_{12}(\mu\text{-bipy})(\text{bipm})_2]$  shows reversible reductions localized in the heterocyclic ligands. No metal-centered reduction is observed. On the contrary, the CV of  $\mathbf{1}\cdot(\text{OTf})_4$  is dominated by the irreversible metal-centered reductions and the reduction of products arising from cathodic decomposition. This could be related to the early onset of the irreversible  $\text{Au}^{\text{I}}$  reduction to  $\text{Au}^0$  at  $-1.2\text{ V}$ , which

(49) Rakhimov, R. D.; Butin, K. P.; Grandberg, K. I. *J. Organomet. Chem.* **1994**, *464*, 253.

(50) Kaim, W.; Schwederski, B.; Dogan, A.; Fiedler, J.; Kuehl, C. J.; Stang, P. J. *Inorg. Chem.* **2002**, *41*, 4025.

(51) Hartmann, H.; Berger, S.; Winter, R.; Fiedler, J.; Kaim, W. *Inorg. Chem.* **2000**, *39*, 4977.

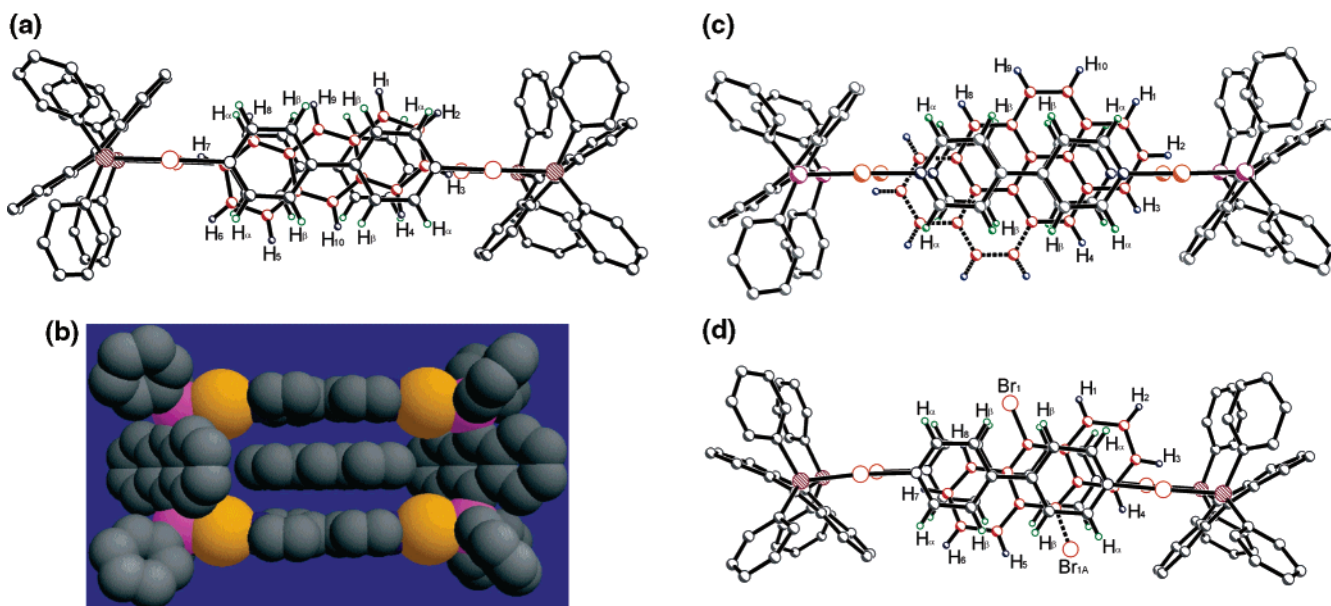


**Figure 5.** (a) Ball-and-stick and (b) space-filling representations of the X-ray crystal structure of  $(1\text{DAn})\cdot(\text{OTf})_4$ , and ball-and-stick representations of the X-ray crystal structures of (c)  $(1\text{DPy})\cdot(\text{OTf})_4\cdot\text{CH}_2\text{Cl}_2$ , and (d)  $(1\text{DBr-An})\cdot(\text{OTf})_4\cdot\text{Et}_2\text{O}$ . Hydrogen atoms and anions are omitted. Color scheme: guest carbon atoms (red), Au (orange), P (purple), guest protons (blue), bipy proton (green).

precedes the bipy-centered reduction at  $-1.38$  V. Our observation is also consistent with the electrochemical properties of most  $\text{Au}^{\text{I}}$ -compounds reported in the literature.<sup>49</sup>

#### X-ray Crystal Structures of the Inclusion Complexes.

Complexation between  $\text{I}^{4+}$  and the aromatic guests was first hinted by the remarkable increase in the solubility of some of the polycyclic molecules such as An and Py in the presence of the gold rectangle, and was further confirmed by the NMR and the luminescence studies (vide infra). Orange crystals of three inclusion complexes  $(1\text{DAn})\cdot(\text{OTf})_4$ ,  $(1\text{DPy})\cdot(\text{OTf})_4\cdot\text{CH}_2\text{Cl}_2$ , and  $(1\text{DBr-An})\cdot(\text{OTf})_4\cdot\text{Et}_2\text{O}$  were obtained by slow diffusion of ether into  $\text{CH}_2\text{Cl}_2/\text{MeOH}$  (8:2, v/v) solutions containing  $\text{I}\cdot(\text{OTf})$  and excess guests; their X-ray crystal structures are shown in Figure 5 (Table 2). The aromatic guests are interposed between the two bipy ligands of the gold rectangle. As commonly observed in the  $\pi$ - $\pi$  stacking of aromatic molecules, the overlap of the aromatic rings of the guests and bipy is staggered.<sup>36</sup> The structures of the compounds confirm the 1:1 host-guest stoichiometry of the complexation.

The An molecule in  $(1\text{DAn})\cdot(\text{OTf})_4$  is intercalated between from the two bipy ligands. The orientation of the guest in the cavity is centrosymmetric with the center of the molecule coinciding with the center of inversion of the host. As a result, the complex shows an approximate  $C_{2h}$  symmetry. Furthermore, the An is oriented with its long  $C_2$  axis close to the N-N vector of the bipy (Figure 5a and Table 2). The small angle  $\tau$  of  $12.4^\circ$  between the axes results in extensive overlap of the aromatic rings of the An and the bipy. The  $\text{H}_{1,5}$  of the guest are protruded slightly out of the periphery of  $\text{I}^{4+}$ , while the rest of its hydrogen atoms are close to the bipy rings. Notably, the  $\text{H}_3$  and  $\text{H}_7$  at the two ends of the guest are found directly pointed toward the lateral rings of the anthracenyl unit. The calculated distance between the  $\text{H}_{3,7}$  and the centroids of the lateral rings is  $2.928$  Å, and the distance between centroids of the lateral ring and the ring containing the interacting hydrogen atoms is  $5.115$  Å. These structural features suggest the presence of weak  $\text{C}-\text{H}\cdots\pi$  or edge-to-face interactions between the guest and the anthracenyl

rings.<sup>52</sup> It is noted that the structures of the inclusion complexes of  $\text{CBPQT}^{4+}$  and hydroquinols show similar  $\text{C}-\text{H}\cdots\pi$  between the guest and the *p*-phenylene rings of the host.<sup>36</sup> The distances ( $2.8$ – $2.9$  Å) between the interacting hydrogen atoms and the *p*-phenylene ring are close to the distance between the  $\text{H}_{3,7}$  and the anthracenyl rings ( $2.928$  Å). The  $\text{H}_\alpha$  and  $\text{H}_\beta$  of the bipy are close to the rings of the An.

The bound Py in  $(1\text{DPy})\cdot(\text{OTf})_4\cdot\text{CH}_2\text{Cl}_2$  is disordered equally over two positions (Figure 5c and Table 2). The  $C_2$  axis of the rectangle passes through the midpoint between the  $\text{C}5\text{a}$  and  $\text{C}5\text{a}^1$  of the Py, which also coincides with the center of the rectangle. The two disordered positions of the Py are generated by a  $180^\circ$  rotation of the guest around the  $C_2$  axis. The guest is located slightly closer to one end of the rectangle than the other. The long  $C_2$  axis of the guest is almost in line with the horizontal N-N axis of the bipy, showing a small angle  $\tau$  of  $0.9^\circ$ . This leads to extensive overlaps between of the Py and bipy rings. The  $\text{H}_{9,10}$  of the Py are protruded out of the cavity of  $\text{I}^{4+}$ , while the rest of the guest protons are close to the bipy. Notably, the  $\text{H}_2$  and  $\text{H}_3$  are directed toward the lateral ring of the anthracenyl backbone. The calculated distance between the centroids of the lateral rings and  $\text{H}_2$  and  $\text{H}_3$  are  $2.673$  and  $3.189$  Å, respectively, and the distance between the centroids of the lateral ring and the axial ring of the Py bearing the two protons is  $4.678$  Å. These structural features compare favorably with the ones reported for edge-to-face interactions,<sup>52</sup> suggesting the presence of the hydrogen bonding between the host and the guest.

The Br-An in  $(1\text{DBr-An})\cdot(\text{OTf})_4\cdot\text{Et}_2\text{O}$  is disordered over two sites A (55% occupancy) and B (45% occupancy), which are related by  $180^\circ$  rotation around the long axis of the molecule (Figure 5d and Table 2). The position of the guest is asymmetric, being closer to one end of the host than the other. The long

(52) (a) Bacon, G. E.; Curry, N. A.; Wilson, S. A. *Proc. R. Soc. London, Ser. A* **1964**, 279, 98. (b) Kelbe, G.; Diederich, F. *Philos. Trans. R. Soc. London, Ser. A* **1993**, 345, 37. (c) Oikawa, S.; Tsuda, M.; Kato, H.; Urabe, T. *Acta Crystallogr., Sect. B* **1985**, 41, 437. (d) Bong, D. T.; Ghadiri, M. R. *Angew. Chem., Int. Ed.* **2001**, 40, 2163. (e) Dance, I.; Scudder, M. *Chem.-Eur. J.* **1996**, 5, 482.

axis of the Br–An and the N–N vector of the bipy is separated by an angle  $\tau$  of 25.9°. In site A, the H<sub>1</sub>, H<sub>2</sub>, H<sub>5</sub>, and H<sub>6</sub> of the guest are protruded out of the rim of the 1<sup>4+</sup> ion, while the H<sub>4</sub> and H<sub>7</sub> are near to the pyridyl rings. The Br atom and its H<sub>10</sub> are projected out of the cavity. The terminal protons of the guest are involved in edge-to-face interactions with the anthracenyl rings as the H<sub>3</sub>–C<sub>3</sub>–C<sub>4</sub>–H<sub>4</sub> edge of the guest is directed toward one of the lateral rings of the anthracenyl backbone. The distances between the H<sub>3</sub> and H<sub>4</sub> and the centroid of the lateral ring are 3.419 and 2.766 Å, respectively. The centroids of the lateral ring and the ring containing the interacting H atoms are separated by 4.846 Å. These structural parameters compare favorably with the aromatic compounds that exhibit similar edge-to-face interactions.<sup>52</sup> The H<sub>α</sub> and H<sub>β</sub> of the bipy are close to the  $\pi$ -rings of the guest. The distances between the Br atom and the H<sub>α</sub> and H<sub>β</sub> of the bipy (3.598–3.841 Å) are too long for C–H···Br hydrogen bonding.

Among all of the structural features of the inclusion complexes, the one of particular importance is the interplanar distance  $d$  between the bipy and the guest, as it is related to the strength of the guest binding. Because the pyridyl rings in the bipy are not coplanar, the interplanar distance is defined as  $d = b - a$  where  $b$  is the perpendicular distance between the  $\alpha$ -carbon atom in the bipy and the plane of the guest, and  $a$  is the perpendicular distance between the carbon atom and the best plane of the bipy (Scheme for Table 2). It is found that the interplanar distances in the three complexes fall into the range of  $\pi$ – $\pi$  interactions ( $\sim 3.5$ – $3.7$  Å) and follow the order of Br–An ( $d = 3.401(4)$  Å) < Py ( $d = 3.552(8)$  Å) < An ( $d = 3.645(2)$  Å). This indicates that the Br–An binds most strongly to 1<sup>4+</sup>, followed by the Py and then the An. It is corroborated by the correlation between the  $d$  and the free energy of binding  $-\Delta G_{\text{NMR}}$  determined by <sup>1</sup>H NMR titration (vide infra), that are 19.7 ± 0.4, 18.2 ± 0.1, and 17.2 ± 0.2 kJ mol<sup>-1</sup> for the binding of the Br–An, Py, and An, respectively. Comparing the dimensions of the 1<sup>4+</sup> ions in the complexes and the free 1<sup>4+</sup> ion in 1·(OTf)<sub>4</sub>·4.8H<sub>2</sub>O shows that the guest binding leads to the shortening of the width of the rectangle: the intraannular Au–Au (6.526(2)–6.854(2) Å), N–N (6.767(4)–7.341(4) Å), and  $\gamma$ -C– $\gamma$ -C = (6.980(4)–7.341(4) Å) distances in the three inclusion complexes are markedly shorter than the ones in the free host: Au–Au = 7.069(3) Å, N–N = 7.665(3) Å, and  $\gamma$ -C– $\gamma$ -C = 7.921(3) Å. Again the intraannular Au–Au, N–N, and  $\gamma$ -C– $\gamma$ -C distances in the three complexes follow the order: Br–An < Py < An. These findings indicate that the guest binding induces contraction of the molecular rectangle, whose extent is proportional to the binding strength of the guests. These observations point to an induced-fit mechanism<sup>53</sup> in which the binding of the guest causes the host to undergo conformational changes which in turn enhance its  $\pi$ – $\pi$  interactions with the guest. The conformation changes involve mainly the contraction of the bite distance of PAnP, which is expected not to be energy demanding as the ligand is highly flexible.<sup>12d,29</sup>

The complexation causes other structural changes in 1<sup>4+</sup> as well. First, the 1<sup>4+</sup> ions in the inclusion complexes are less bulged than the free 1<sup>4+</sup>, showing a smaller angle  $\chi$  of 10.5–

13.2° (cf.  $\chi = 16.8^\circ$  for the free 1<sup>4+</sup>). In addition, the bipy in the complexes are less twisted as the twist angles  $\theta$  for the Br–An- (2.71°), Py- (3.60°), and An-(10.42°) complexes are significant smaller than that for the free host ( $\theta = 21.69^\circ$ ). Similarly, the binding of 1,4-dimethoxybenzene to the CBPQT<sup>4+</sup> ion reduces the twist angle of the bipy units from 19° to 4°.<sup>36a,b</sup> Apparently, the flattening of the bipy would improve the overlap with the aromatic guests and thus enhance the  $\pi$ – $\pi$  interactions. Analogous to the width of the 1<sup>4+</sup> ion, the decrease in the twist angle  $\theta$  observed in the three complexes is in line with the increase in the  $-\Delta G_{\text{NMR}}$ . This observation lends support to the induced-fit mechanism.

Similar to the free host ( $\varpi = 43.7^\circ$ ), the anthracenyl rings in the An- and Py-complexes are tilted toward the same direction with tilt angles  $\varpi$  of 43.3° (An-complex) and 47.4° (Py-complex). In addition, the rings are slightly curved with the dihedral angles  $\epsilon$  of 14.7° (An-complex) and 21.9° (Py-complex). The binding of the guests leads to significant shortening of the intrannular P–P distances. To sustain such a short P–P distance, the central rings in the anthracenyl units are distorted from planarity and the bow angles  $\phi$  in the An- (30.5°) and Py-complexes (31.4°) are markedly larger than that in the free host (22.3°). The 1<sup>4+</sup> ion in the Br–An complex shows a different conformation in which the anthracenyl rings are titled in opposite directions (Figure 5d). Moreover, the two ends of the rectangle are nonequivalent, having slightly different intraannular Au–Au (6.526(2), 6.604(2) Å), and N–N (6.767(4), 6.910(4) Å) distances. As a result, the symmetry of the 1<sup>4+</sup> ion descends to C<sub>s</sub> where the plane of reflection bisects the anthracenyl rings. The intrannular P–P distance (6.255(4) Å) is the shortest among the four gold compounds and is maintained by severe distortion of the central ring of the anthracenyl backbone ( $\phi = 40^\circ$ ).

**Solid-State Self-Assembly.** The crystal structure of 1·(OTf)<sub>4</sub>·4.8H<sub>2</sub>O reveals linear stacking of the 1<sup>4+</sup> ions along the  $c$ -axis, which results in open channels (Figure 6). Similar open channels have been observed in the crystals of [Pt<sub>4</sub>(dppp)<sub>4</sub>( $\mu$ -bipy)<sub>4</sub>]<sup>8+</sup> (dppp = 1,3-bis(diphenylphosphino)propane)<sup>8c,d</sup> and CBPQT<sup>4+</sup>.<sup>36a</sup> The distance between two adjacent Au atoms in a column is 10.308 Å. Sandwiched between two 1<sup>4+</sup> ions are four OTf<sup>-</sup> ions whose CF<sub>3</sub>-groups are pointed toward the center of the rectangle, and the oxygen atoms of the SO<sub>3</sub>-groups are near the  $\alpha$ -H of the pyridyl rings. There are on average 4.8 H<sub>2</sub>O molecules per 1<sup>4+</sup> ion, two of them are found between two stacking 1<sup>4+</sup> ions, and the remaining are located in the interstitial space. The water molecules could be originated from the solvents used in crystal growing, such as MeOH.

The solid-state packing of the 1<sup>4+</sup> ions reveals intriguing tectonic supramolecular arrangement: the 1<sup>4+</sup> ions, paneled on the  $ab$ -plane, form a 2D mosaic in which each ion is surrounded at its corners by four neighboring ions (Figure 6). The packing leads to highly porous crystal with a large interstitial space, which resembles an open channel, located in the center of four adjacent stacking columns of the 1<sup>4+</sup> ions. Viewing down the  $c$ -axis, one would see the two Ph<sub>ax</sub> rings at the “head” of the 1<sup>4+</sup> ion are projected upward, whereas the two Ph<sub>ax</sub> rings are pointing down at the “tail”. The equatorial Ph rings at the head are tilted upward, while the ones at the tail are tilted downward. The axial and equatorial Ph rings in the head and tail are labeled Ph<sub>ax</sub><sup>h</sup>, Ph<sub>eq</sub><sup>h</sup>, Ph<sub>ax</sub><sup>t</sup>, and Ph<sub>eq</sub><sup>t</sup>. In the panel, the head and tail of

(53) (a) Kasai, K.; Aoyagi, M.; Fujita, M. *J. Am. Chem. Soc.* **2000**, *122*, 2140. (b) Fujita, M.; Nagao, S.; Ogura, K. *J. Am. Chem. Soc.* **1995**, *117*, 1649. (c) Hamilton, A. D.; Van Engen, D. *J. Am. Chem. Soc.* **1987**, *109*, 5035. (d) Sijbesma, R. P.; Wijmenga, S. S.; Nolte, R. J. M. *J. Am. Chem. Soc.* **1992**, *114*, 9807. (e) Koshland, D. E., Jr. *Angew. Chem., Int. Ed. Engl.* **1995**, *33*, 2375.

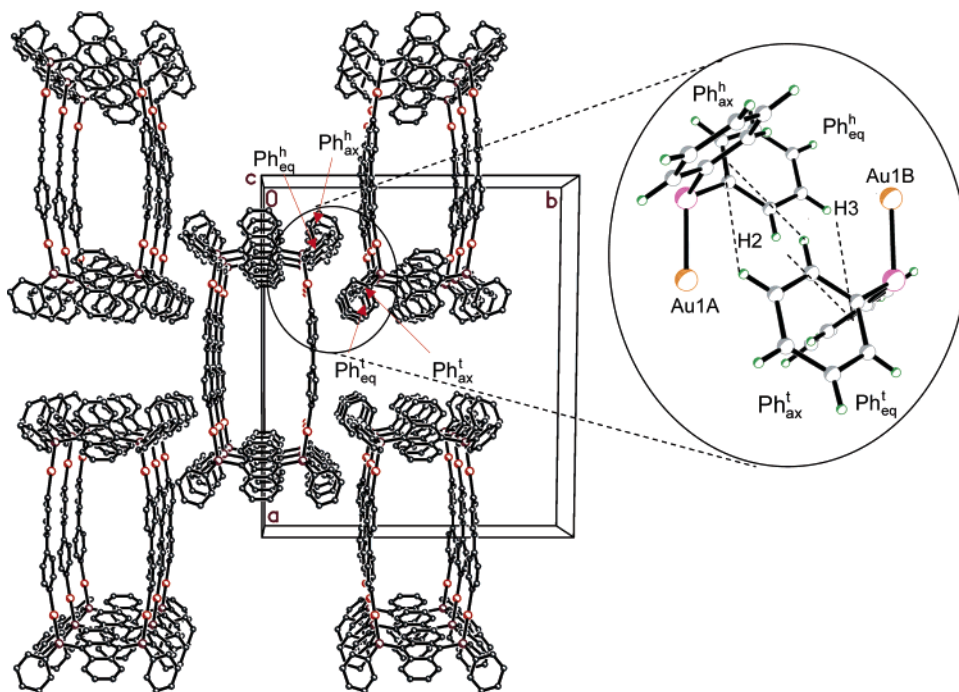


**Figure 6.** Crystal packing diagram of  $1 \cdot (\text{OTf})_4 \cdot 4.8\text{H}_2\text{O}$  showing the open channels and the 2D mosaic on the  $ab$ -plane. Hydrogen atoms, anions, and  $\text{H}_2\text{O}$  molecules are omitted. Inset shows the complementary edge-to-face Ph–Ph interactions between adjacent  $1^{4+}$  ions. Color scheme: see Figure 5.

**Table 3.** Structural Parameters for the Edge-to-Face Ph–Ph Interactions

| complexes   | $1 \cdot (\text{OTf})_4 \cdot 4.8\text{H}_2\text{O}$ | $(1\text{-An}) \cdot (\text{OTf})_4$ | $(1\text{-Py}) \cdot (\text{OTf})_4 \cdot \text{CH}_2\text{Cl}_2$ | $(1\text{-Br-An}) \cdot (\text{OTf})_4 \cdot \text{Et}_2\text{O}$ |
|---|--|--------------------------------------|---|---|
| $i$ (Å)   | 4.988  | 4.900                                | 4.954   | 5.078, 5.316  |
| $j$ (Å)   | 3.496, 3.279   | 3.484, 3.279                         | 3.438, 3.395  | 3.312, 3.493, 3.518, 3.629  |
| $k$ (Å)   | 6.025  | 5.996                                | 5.962   | 5.995   |
| dihedral angle  | 87.8   | 89.0                                 | 89.4  | 88.1, 89.9  |
| dihedral angle between $\text{Ph}_{\text{ax}}^{\text{h}}$ and $\text{Ph}_{\text{ax}}^{\text{t}}$ or $\text{Ph}_{\text{eq}}^{\text{h}}$ and $\text{Ph}_{\text{eq}}^{\text{t}}$ | 0.0  | 0.0                                  | 0.0   | 7.9, 5.4  |

a rectangle are next to the tails and the heads of its neighboring molecules, respectively. This head-to-tail orientation allows complementary edge-to-face interactions of the Ph rings between adjacent molecules: the  $\text{Ph}_{\text{ax}}^{\text{h}}$  rings of a rectangle are faced directly to the edges of the  $\text{Ph}_{\text{eq}}^{\text{t}}$  rings of two molecules in the front. Conversely, the edges of  $\text{Ph}_{\text{eq}}^{\text{h}}$  rings of the rectangle are directed toward the faces of  $\text{Ph}_{\text{ax}}^{\text{t}}$  rings of the two preceding molecules (inset in Figure 6). These complementary  $\text{Ph}_{\text{ax}}^{\text{h}}-\text{Ph}_{\text{eq}}^{\text{t}}$  and  $\text{Ph}_{\text{ax}}^{\text{t}}-\text{Ph}_{\text{eq}}^{\text{h}}$  interactions occur at every corner in the mosaic. The  $\text{H}_2$  and  $\text{H}_3$  in the  $\text{Ph}_{\text{eq}}^{\text{t}}/\text{Ph}_{\text{eq}}^{\text{h}}$  ring are directed toward the centroid of the  $\text{Ph}_{\text{ax}}^{\text{h}}/\text{Ph}_{\text{ax}}^{\text{t}}$  with the calculated  $\text{H} \cdots$ centroid distances  $j$  of 3.496 and 3.279 Å (Table 3, for the definitions of structural parameters, see Scheme for Table 3). The interacting Ph rings are almost perpendicular to each other, showing a dihedral angle of 87.8°. The distance ( $i$ ) between their centroids

is 4.988 Å. The intermolecular P–P distance ( $k$ ) between the two interacting  $\text{PPh}_2$  groups is 6.025 Å. As demonstrated by the comprehensive surveys of Dance and Scudder, edge-to-face Ph–Ph interactions, also known as “phenyl embrace”, widely occur in the crystals of metal complexes containing  $\text{PPh}_3$  or diphosphines, such as  $\text{PPh}_2\text{CH}_2\text{PPh}_2$  as ligands, and have a determining effect on the solid-state packing of the complexes.<sup>52e,54</sup> The values of  $i$  and  $k$  observed in  $1 \cdot (\text{OTf})_4 \cdot 4.8\text{H}_2\text{O}$  fall into the average values of  $i$  (5 Å) and  $k$  ( $\leq 7$  Å) obtained from the surveys. In addition, the dihedral angle (87.8°) and the  $i$  value (4.988 Å) of the gold complex compare favorably

(54) (a) Dance, I.; Scudder, M. *J. Chem. Soc., Chem. Commun.* **1995**, 1039. (b) Dance, I.; Scudder, M. *J. Chem. Soc., Dalton Trans.* **2000**, 1579. (c) Dance, I.; Scudder, M. *J. Chem. Soc., Dalton Trans.* **2000**, 1587. (d) Scudder, M.; Dance, I. *J. Chem. Soc., Dalton Trans.* **1998**, 3167. (e) Dance, I.; Scudder, M. *J. Chem. Soc., Dalton Trans.* **1998**, 1341.

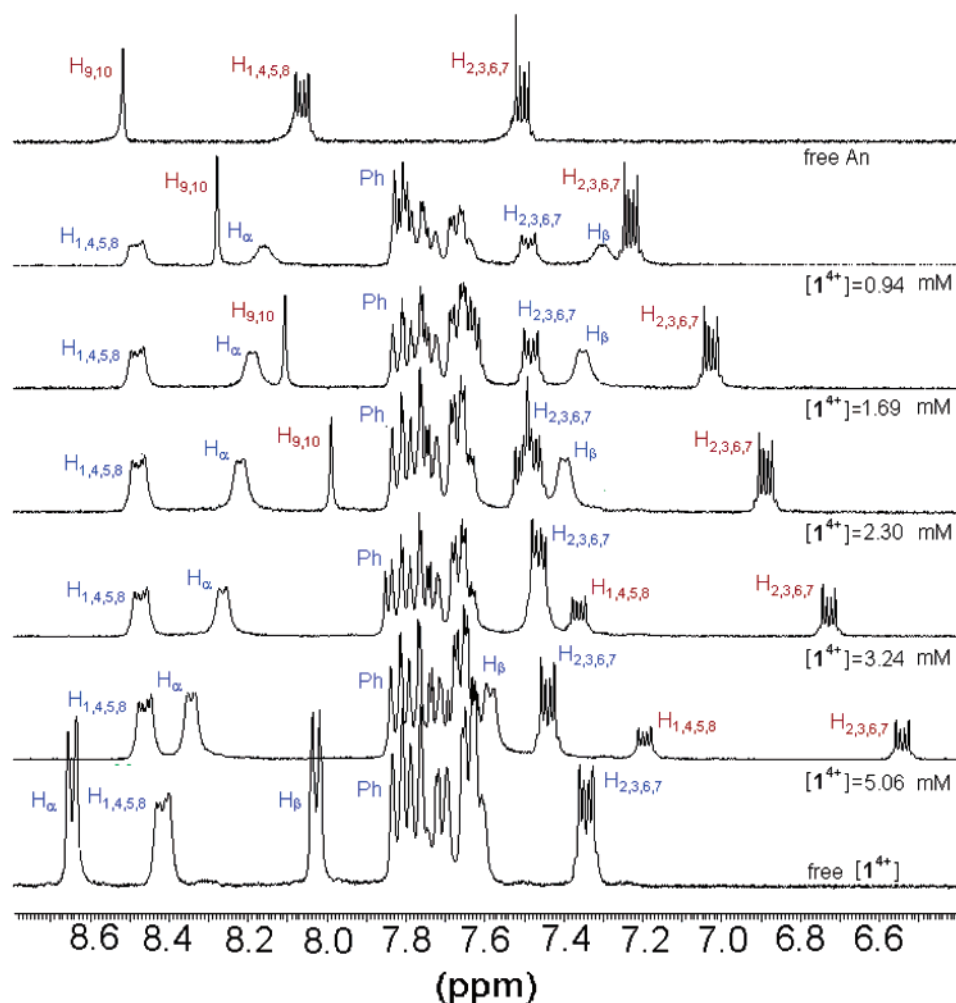


**Figure 7.**  $^1\text{H}$  NMR spectral change upon addition of  $\mathbf{1}\cdot(\text{OTf})_4$  (concentration = 0.00–5.06 mM) to a  $\text{CD}_3\text{CN}$  solution of An (concentration = 2.52 mM). The  $\mathbf{1}\cdot(\text{OTf})_4$  and An protons are labeled in blue and red, respectively. The top and bottom spectra belong to the free An and the free  $\mathbf{1}\cdot(\text{OTf})_4$ , respectively. The shifts of the host protons increase as the  $[\text{H}]_t$  decreases because when the  $[\text{G}]_t$  is fixed the percentage of occupied host increases as  $[\text{H}]_t$  is lowered.

with the corresponding parameters between a pair of benzene molecules engaging in edge-to-face interactions (dihedral angle =  $86.5^\circ$ ,  $i = 5.025 \text{ \AA}$ ).<sup>52a–c</sup> It is believed that the complementary edge-to-face Ph–Ph interactions are a major driving force for the self-assembly of  $\mathbf{1}^{4+}$  in the solid state.

Reminiscent of the free host, the  $\mathbf{1}^{4+}$  ions in the solids of An- and Py-complexes form linear channels and assembled into 2D mosaic via the complementary interactions of the nearly perpendicular  $\text{Ph}_{\text{ax}}^{\text{h}}\text{--Ph}_{\text{eq}}^{\text{t}}$  and  $\text{Ph}_{\text{ax}}^{\text{t}}\text{--Ph}_{\text{eq}}^{\text{h}}$  rings (Figures S24, 25). The  $i$ ,  $j$ , and  $k$  distances are comparable with the ones observed in  $\mathbf{1}\cdot(\text{OTf})_4\cdot 4.8\text{H}_2\text{O}$  (Table 3). The channels are occupied by the guests, and the separations of  $\mathbf{1}^{4+}$  ions in the columns and the positions of anions are similar to those in  $\mathbf{1}\cdot(\text{OTf})_4\cdot 4.8\text{H}_2\text{O}$ . The  $\text{CH}_2\text{Cl}_2$  molecules in  $(\mathbf{1}\supset\text{Py})\cdot(\text{OTf})_4\cdot\text{CH}_2\text{Cl}_2$  are sandwiched between the stacking  $\mathbf{1}^{4+}$  ions.

On the other hand, the  $\mathbf{1}^{4+}$  ions in the Br–An-complex form zigzag-like columns (Figure S26). Sandwiched between two stacking gold rectangles are one  $\text{CH}_2\text{Cl}_2$  molecule and four  $\text{OTf}^-$  ions. While the  $\mathbf{1}^{4+}$  ions in the Br–An-complex self-assemble into a 2D mosaic similar to those observed in the other three complexes, there are some subtle differences. Unlike the other three gold complexes, the anthracenyl rings in the Br–An-complex are tilted toward each other (Figure 5d). As a consequence, the four  $\text{Ph}_{\text{ax}}$  rings at both ends of the rectangle are pointing

upward, while the four  $\text{Ph}_{\text{eq}}$  rings are tilted downward. It is apparent that if all of the  $\mathbf{1}^{4+}$  ions in the panel have the same orientation, complementary  $\text{Ph}_{\text{ax}}\text{--Ph}_{\text{eq}}$  interactions as observed in the other three compounds would not be possible. It is therefore intriguing to find that each rectangle in the Br–An-complex is surrounded by four “flipped-over” rectangles whose orientation is different from that of the surrounded ion by a  $180^\circ$  rotation around the long central axis (Figure S27). As such, the four upward pointed  $\text{Ph}_{\text{ax}}$  rings of the surrounded rectangle now face directly to the four upward tilted  $\text{Ph}_{\text{eq}}$  of its neighbors. Conversely, the downward pointed  $\text{Ph}_{\text{ax}}$  rings of the four adjacent molecules face to the edges of the downward tilted  $\text{Ph}_{\text{eq}}$  rings of the central molecule. The interacting Ph rings are nearly perpendicular to each other, and the  $i$ ,  $j$ , and  $k$  distances are close to those found in the other three compounds (Table 3). The special arrangement of the  $\mathbf{1}^{4+}$  ions in the crystal of the Br–An-complex underscores the important role played by the complementary edge-to-face  $\text{Ph}_{\text{ax}}\text{--Ph}_{\text{eq}}$  interactions in the solid-state self-assembly of the gold complex.

**$^1\text{H}$  NMR Titrations.** The complexation between  $\mathbf{1}^{4+}$  and the guest was investigated by monitoring chemical shifts  $\delta_{\text{G}}$  of certain guest protons as a function of the total concentration of the host  $[\text{H}]_t$ . Figure 7 shows the spectroscopic changes observed in the titration of  $\mathbf{1}\cdot(\text{OTf})_4$  and An. Invariably, the complexation

**Table 4.** Binding Constants and Free Energy of Binding for the Aromatic Guests Determined by  $^1\text{H}$  NMR and Fluorescence Titrations

| guest                    | $K_{\text{NMR}} (\text{M}^{-1})$ | $-\Delta G_{\text{NMR}} (\text{kJ mol}^{-1})$ | $K_{\text{G}} (\text{M}^{-1})$ | $-\Delta G_{\text{G}} (\text{kJ mol}^{-1})$ |
|--------------------------|----------------------------------|---|--------------------------------|---|
| Dmb                      | $50 \pm 7$                       | $9.7 \pm 0.4$                                 | a                              |   |
| Bip                      | $126 \pm 10$                     | $12.0 \pm 0.2$                                | a                              |   |
| Nap                      | $128 \pm 52$                     | $12.0 \pm 1.0$                                | $118 \pm 31$                   | $11.8 \pm 0.7$                              |
| Phen                     | $527 \pm 26$                     | $15.5 \pm 0.1$                                | $463 \pm 29$                   |   |
| An                       | $1029 \pm 71$                    | $17.2 \pm 0.2$                                | $909 \pm 103$                  | $16.9 \pm 0.3$                              |
| MeO-An                   | $1353 \pm 70$                    | $17.9 \pm 0.1$                                | b                              |   |
| NC-An                    | $1137 \pm 32$                    | $17.4 \pm 0.1$                                | b                              |   |
| Br-An                    | $2858 \pm 508$                   | $19.7 \pm 0.4$                                | $2277 \pm 160$                 | $19.2 \pm 0.2$                              |
| $\text{CO}_2\text{H-An}$ | $2559 \pm 350$                   | $19.4 \pm 0.3$                                | $2208 \pm 223$                 | $19.1 \pm 0.3$                              |
| Py                       | $1564 \pm 34$                    | $18.2 \pm 0.1$                                | $1376 \pm 40$                  | $17.9 \pm 0.1$                              |

<sup>a</sup> No quenching. <sup>b</sup> Cannot be determined as the emissions of the guests and the host overlap.

moves all of the guest protons, and the  $\text{H}_{\alpha}$  and  $\text{H}_{\beta}$  of bipy upfield but the  $\text{H}_{1,4,5,8}$  and  $\text{H}_{2,3,6,7}$  of the anthracenyl rings in the host downfield (Figures S28–36). That all of the guest protons and the  $\text{H}_{\alpha}$  and  $\text{H}_{\beta}$  of the bipy are shifted upfield indicates the participation of the bipy in the guest binding. It is in accordance with the inclusion geometries exhibited by the three complexes. The upfield shifts are attributable to the influence of the diatropic ring currents of the aromatic rings. Similar upfield shifts have been observed in the binding of aromatic guests to the CBPQT<sup>4+</sup> ion.<sup>36</sup>

Except the  $\text{H}_{\alpha}$  and  $\text{H}_{\beta}$ , which are slightly broadened, the signals of all of the guest and host protons remain sharp throughout the titrations. This implies that the guest exchanges rapidly between the cavity of  $1^{4+}$  and the solution in the NMR time scale. Thus, the observed chemical shifts of the guest protons ( $\delta_{\text{G}}$ ) are the weighted average of the chemical shifts of the complexed guest  $\delta_{\text{G}}^{\text{C}}$  and the free guest  $\delta_{\text{G}}^{\text{F}}$ . The stoichiometry of the inclusion complexes was established to be 1:1 by Job's plots (Figures S37–46). The binding constants  $K_{\text{NMR}}$  and the chemical shift differences  $\Delta\delta_{\text{G}}$  ( $\Delta\delta_{\text{G}} = \delta_{\text{G}}^{\text{C}} - \delta_{\text{G}}^{\text{F}}$ ) are obtained from the least-squares fit (Figures S47–56) to eq 1,<sup>40</sup> where  $[G]_{\text{t}}$  is the total concentration of the guest.

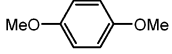
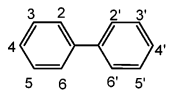
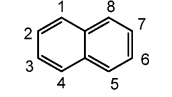
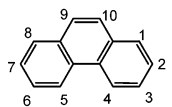
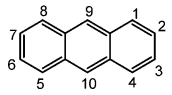
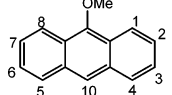
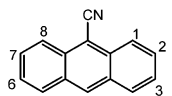
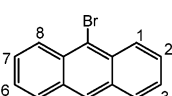
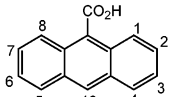
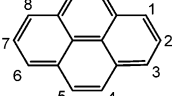
$$\delta_{\text{G}} = \delta_{\text{G}}^{\text{F}} - \left( \frac{\Delta\delta_{\text{G}}}{2[G]_{\text{t}}} \right) (B - \sqrt{B^2 - 4[H]_{\text{t}}[G]_{\text{t}}}) \quad (1)$$

$$B = [H]_{\text{t}} + [G]_{\text{t}} + \frac{1}{K_{\text{NMR}}} \quad (1.1)$$

The binding constants  $K_{\text{NMR}}$  of the aromatic guests differ greatly, ranging from  $50 \pm 7 \text{ M}^{-1}$  for Dmb to  $2858 \pm 508 \text{ M}^{-1}$  for Br-An. The  $K_{\text{NMR}}$  and the free energy of the binding  $-\Delta G_{\text{NMR}}$  are listed in Table 4.

**Chemical Shift Differences Induced by Binding.** Other parameters extracted from the least-squares fit are the chemical shifts differences of the guest ( $\Delta\delta_{\text{G}}$ ) and host ( $\Delta\delta_{\text{H}}$ ) protons induced by the complexation (Table 5). It is noted that the  $\Delta\delta_{\text{G}}$  values roughly correlate with the binding free energy  $-\Delta G_{\text{NMR}}$ ; that is, the weakly binding Dmb, Bip, and Nap ( $-\Delta G_{\text{NMR}} = 9.7\text{--}12.0 \text{ kJ mol}^{-1}$ ) show  $\Delta\delta_{\text{G}}$  values ( $-0.16$  to  $-0.76 \text{ ppm}$ ) that are markedly smaller than those observed for the Phen, An, 9-substituted anthracenes, and Py ( $-\Delta G_{\text{NMR}} = 15.5\text{--}19.7 \text{ kJ mol}^{-1}$ ,  $\Delta\delta_{\text{G}} = -0.65$  to  $-1.68 \text{ ppm}$ ). The same trend is observed in the  $\Delta\delta_{\text{H}}$  for the  $\text{H}_{\alpha}$  and  $\text{H}_{\beta}$ : for example, the binding of Dmb, Bip, and Nap induces upfield shifts of the  $\text{H}_{\beta}$  ( $\Delta\delta_{\text{H}} = -0.07$  to  $-0.11 \text{ ppm}$ ) that are remarkably smaller than those

**Table 5.** Chemical Shifts ( $\delta$ ) of the Free Host and Guest Protons and the Change in the Chemical Shifts ( $\Delta\delta$ ) Induced by the Complexation

| Guest  | Guest Protons          |          |                           | Host Protons         |                           |
|--|------------------------|----------|---------------------------|----------------------|---------------------------|
|  | H                      | $\delta$ | $\Delta\delta_{\text{G}}$ | H                    | $\Delta\delta_{\text{H}}$ |
|    | $\text{H}_{2,3,5,6}$   | 6.85     | -0.32                     | $\text{H}_{\alpha}$  | 0.00                      |
|  | $\text{H}_{\text{Me}}$ | 3.73     | -0.16                     | $\text{H}_{\beta}$   | -0.07                     |
|    | $\text{H}_{2,2',6,6'}$ | 7.63     | -0.76                     | $\text{H}_{\alpha}$  | -0.04                     |
|  | $\text{H}_{3,3',5,5'}$ | 7.46     | -0.47                     | $\text{H}_{\beta}$   | -0.11                     |
|  | $\text{H}_{4,4'}$      | 7.37     | -0.45                     | $\text{H}_{1,4,5,8}$ | 0.00                      |
|    | $\text{H}_{1,4,5,8}$   | 7.91     | -0.31                     | $\text{H}_{\alpha}$  | -0.02                     |
|  | $\text{H}_{2,3,6,7}$   | 7.29     | -0.25                     | $\text{H}_{\beta}$   | -0.09                     |
|  |                        |          |                           | $\text{H}_{1,4,5,8}$ | 0.00                      |
|    | $\text{H}_{4,5}$       | 8.79     | -1.14                     | $\text{H}_{\alpha}$  | -0.29                     |
|  | $\text{H}_{9,10}$      | 7.81     | -0.81                     | $\text{H}_{\beta}$   | -0.62                     |
|  | $\text{H}_{3,6}$       | 7.95     | a                         | $\text{H}_{1,4,5,8}$ | +0.04                     |
|  | $\text{H}_{2,7}$       | 7.67     | -1.37                     | $\text{H}_{2,3,6,7}$ | +0.10                     |
|  | $\text{H}_{1,8}$       | 7.73     | -0.88                     |                      |                           |
|    | $\text{H}_{9,10}$      | 8.52     | -1.16                     | $\text{H}_{\alpha}$  | -0.61                     |
|  | $\text{H}_{1,4,5,8}$   | 8.08     | -1.15                     | $\text{H}_{\beta}$   | -0.90                     |
|  | $\text{H}_{2,3,6,7}$   | 7.52     | -1.40                     | $\text{H}_{1,4,5,8}$ | +0.08                     |
|  | $\text{H}_{10}$        | 8.31     | -1.28                     | $\text{H}_{\alpha}$  | -0.66                     |
|  | $\text{H}_{1,8}$       | 8.29     | a                         | $\text{H}_{\beta}$   | -0.94                     |
|  | $\text{H}_{4,5}$       | 8.05     | a                         | $\text{H}_{1,4,5,8}$ | +0.08                     |
|  | $\text{H}_{2,3,6,7}$   | 7.52     | -1.20                     | $\text{H}_{2,3,6,7}$ | +0.14                     |
|  | $\text{H}_{\text{Me}}$ | 4.13     | -0.39                     |                      |                           |
|  | $\text{H}_{10}$        | 8.90     | -0.83                     | $\text{H}_{\alpha}$  | -0.55                     |
|  | $\text{H}_{1,8}$       | 8.40     | -1.06                     | $\text{H}_{\beta}$   | -0.87                     |
|  | $\text{H}_{4,5}$       | 8.23     | a                         | $\text{H}_{1,4,5,8}$ | +0.08                     |
|  | $\text{H}_{2,7}$       | 7.81     | a                         | $\text{H}_{2,3,6,7}$ | +0.13                     |
|  | $\text{H}_{3,6}$       | 7.67     | -1.16                     |                      |                           |
|  | $\text{H}_{10}$        | 8.62     | -0.84                     | $\text{H}_{\alpha}$  | -0.66                     |
|  | $\text{H}_{1,8}$       | 8.52     | a                         | $\text{H}_{\beta}$   | -0.97                     |
|  | $\text{H}_{4,5}$       | 8.10     | -0.97                     | $\text{H}_{1,4,5,8}$ | +0.01                     |
|  | $\text{H}_{2,7}$       | 7.71     | a                         | $\text{H}_{2,3,6,7}$ | +0.19                     |
|  | $\text{H}_{3,6}$       | 7.56     | -1.10                     |                      |                           |
|  | $\text{H}_{10}$        | 8.67     | -0.82                     | $\text{H}_{\alpha}$  | -0.70                     |
|  | $\text{H}_{1,8}$       | 8.14     | a                         | $\text{H}_{\beta}$   | -0.90                     |
|  | $\text{H}_{4,5}$       | 8.11     | -1.25                     | $\text{H}_{1,4,5,8}$ | +0.09                     |
|  | $\text{H}_{2,3,6,7}$   | 7.57     | -1.39                     | $\text{H}_{2,3,6,7}$ | +0.19                     |
|  | $\text{H}_{1,3,6,8}$   | 8.25     | -1.19                     | $\text{H}_{\alpha}$  | -0.80                     |
|  | $\text{H}_{4,5,9,10}$  | 8.15     | -0.65                     | $\text{H}_{\beta}$   | -1.47                     |
|  | $\text{H}_{2,7}$       | 8.06     | -1.68                     | $\text{H}_{1,4,5,8}$ | +0.10                     |
|  |                        |          |                           | $\text{H}_{2,3,6,7}$ | +0.21                     |

<sup>a</sup> Cannot be determined as the signals are masked.

elicited by the binding of the other guests ( $\Delta\delta_{\text{H}} = -0.62$  to  $-1.47 \text{ ppm}$ ). As discussed in the previous section, the increase in  $-\Delta G_{\text{NMR}}$  reduces the interplanar distance between the bipy ligands and the guest. It is reasonable to expect that the decrease in separation would lead to stronger mutual shielding which in turn gives rise to the larger  $\Delta\delta_{\text{G}}$  and  $\Delta\delta_{\text{H}}$  values observed.

The  $\Delta\delta_G$  values of the protons in a guest are dependent on the inclusion geometry, the distance between the protons and the bipy, and the intrinsic susceptibility of the protons.<sup>36c,55</sup> In general, the  $\Delta\delta_G$  values of the protons in the three inclusion complexes are in accordance with their X-ray crystal structures, suggesting that the solid-state inclusion geometries could represent the time-averaged orientation of the bound guests in solution.

First, all of the protons in the An show similar large  $\Delta\delta_G$  values of  $-1.15$  to  $-1.40$  ppm (Table 5), consistent with the extensive overlap between the aromatic rings of An and bipy observed in the structure of the An-complex. Although the H<sub>1,5</sub> and H<sub>4,8</sub>, H<sub>9</sub> and H<sub>10</sub>, and H<sub>2,6</sub> and H<sub>3,7</sub> are nonequivalent in the solid-state structure, only three sets of multiplets corresponding to H<sub>1,4,5,8</sub>, H<sub>9,10</sub>, and H<sub>2,3,6,7</sub> are found in the solution NMR spectrum of **1**<sup>4+</sup> and An mixture (Figure 7). The coalescence of the signals is due to rapid rotation of the guest inside the host and/or fast exchange between the bound and free guest molecules. Notably, the  $\Delta\delta_G$  value for the H<sub>2,3,6,7</sub> ( $-1.40$  ppm) is slightly larger than the  $\Delta\delta_G$  values of the other protons ( $-1.15$  ppm). This could be due to the edge-to-face interactions between the anthracenyl rings and the protons, or the shielding of the terminal protons by the diatropic current of the anthracenyl rings. Similarly, the hydroquinols protons involved in edge-to-face interactions with the *p*-phenylene rings of CBPQT<sup>4+</sup> are more upfield shifted than the other protons.<sup>36c</sup>

The complexation between Py and the gold rectangle leads to a large upfield shift of the apical H<sub>2,7</sub> ( $\Delta\delta_G = -1.68$  ppm) (Table 5). It can be aptly accounted by the solid-state orientation of the guest where the H<sub>7</sub> is covered by two pyridyl rings and the H<sub>2</sub> is engaged in edge-to-face interactions with the anthracenyl ring.<sup>36c</sup> The H<sub>1,3,6,8</sub> shows a smaller  $\Delta\delta_G$  value as they are not so close to the bipy and anthracenyl rings. The H<sub>4,5,9,10</sub>, which are protruded out of the rim of the rectangle, show the smallest  $\Delta\delta_G$  value of  $-0.65$  ppm.

The  $\Delta\delta_G$  values for the Br–An protons can also be correlated with the solid-state inclusion geometry of the complex (Table 5). The H<sub>10</sub>, which is far from the cavity, is less shielded ( $\Delta\delta_G = -0.84$  ppm) than the other protons. The  $\Delta\delta_G$  values for H<sub>1,8</sub> and H<sub>2,7</sub> cannot be determined as they are masked by the other signals. The H<sub>4,5</sub> ( $-0.97$  ppm) and H<sub>3,6</sub> ( $-1.10$  ppm) show similar large  $\Delta\delta_G$  values, which are reasonable as these protons are close to the bipy and involved in the edge-to-face interactions with the anthracenyl rings. Similarly, the terminal H<sub>2,7</sub> and H<sub>3,6</sub> of NC–An and CO<sub>2</sub>H–An are more shielded than the H<sub>10</sub>.

The methoxyl protons in Dmb ( $\Delta\delta_G = -0.16$  ppm) and MeO–An ( $\Delta\delta_G = -0.39$  ppm) are much less affected by the binding than the aromatic protons of the compounds ( $\Delta\delta_G = -0.32$  ppm for Dmb and  $\Delta\delta_G = -1.20$  and  $-1.28$  ppm for MeO–An) (Table 5). The small  $\Delta\delta$  values displayed by the methoxyl protons reflect their long separations from the  $\pi$ -rings of the bipy. In view of the structures of the three inclusion complexes, one would expect the binding involves mainly the aromatic rings of Dmb and MeO–An, and their methoxyl groups could be projected out of the rims of the **1**<sup>4+</sup> ion.

The binding also moves the resonances of the H <sub>$\beta$</sub>  and H <sub>$\alpha$</sub>  of the bipy to higher field. In all cases, the H <sub>$\beta$</sub>  ( $\Delta\delta_H = -0.87$  to

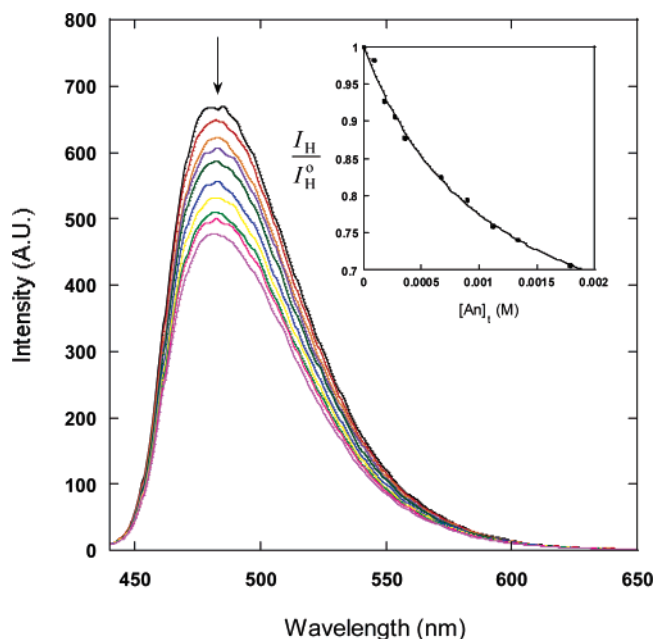


**Figure 8.** Emission spectral change upon addition of An to a CH<sub>3</sub>CN solution of **1**•(OTf)<sub>4</sub>. Excitation wavelength = 420 nm, excitation and emission slit width = 10 nm. Inset shows the emission titration curve and the least-squares fit using the eq 2. The emission intensity of the host is monitored at 480 nm.

$-1.47$  ppm) are more affected than the H <sub>$\alpha$</sub>  ( $\Delta\delta_H = -0.55$  to  $-0.80$  ppm) (Table 5). It is reasonable, as the H <sub>$\beta$</sub> , being closer than H <sub>$\alpha$</sub>  to the central position, would be more shielded by the  $\pi$ -rings of the guests. Unlike the bipy protons, the protons of the anthracenyl rings are downfield shifted upon the complexation. And invariably, the H<sub>2,3,6,7</sub> are more affected ( $\Delta\delta_H = 0.01$ – $0.21$  ppm) than the H<sub>1,4,5,8</sub> ( $\Delta\delta_H = 0.00$ – $0.10$  ppm) at the ends of the ring. The downfield shifts could be due to the distortion of the anthracenyl ring caused by the binding. Another possible cause is the interactions of the rings with the apical protons of the guests. Similarly, downfield shifts of the *p*-phenylene rings of the CBPQT<sup>4+</sup> ion upon binding of hydroquinols were also accounted for by edge-to-face interactions between the protons of the hydroquinols and the *p*-phenylene rings.<sup>36c</sup>

**Fluorescence Quenching of the Host.** The emission of **1**<sup>4+</sup> at 480 nm is quenched by Nap, Phen, An, Br–An, CO<sub>2</sub>H–An, MeO–An, NC–An, and Py (Figures S57–60). However, the fluorescence intensity is not diminished even in the presence of a large excess of Dmb and Bip. Figure 8 shows the change of the emission intensity of **1**<sup>4+</sup> upon addition of An. The binding constants  $K_Q$  for the guests were determined from the least-squares fits to the eq 2<sup>41</sup> for 1:1 host–guest complexation (Figures S61–65).

$$\frac{I_H}{I_H^0} = \frac{1 + \left(\frac{k_{H-G}}{k_H}\right)K_Q[G]_t}{1 + K_Q[G]_t} \quad (2)$$

The  $K_Q$  values for MeO–An and NC–An are not determined, as the emission of the guests overlaps with that of **1**<sup>4+</sup>. The  $K_Q$  and the binding free energy  $-\Delta G_Q$  are listed in Table 4. The results show that the  $K_Q$  values are close to the corresponding  $K_{NMR}$  values determined from <sup>1</sup>H NMR titrations. This leads to the conclusion that the quenching only occurs when the guest

(55) (a) Odashima, K.; Itai, A.; Iitaka, Y.; Arata, Y.; Koga, K. *Tetrahedron Lett.* **1980**, 21, 4347. (b) Diederich, F.; Griebel, D. *J. Am. Chem. Soc.* **1984**, 106, 8037. (c) Cowart, M. D.; Sucholeiki, I.; Bukownik, R. R.; Wilcox, C. S. *J. Am. Chem. Soc.* **1988**, 110, 6204.



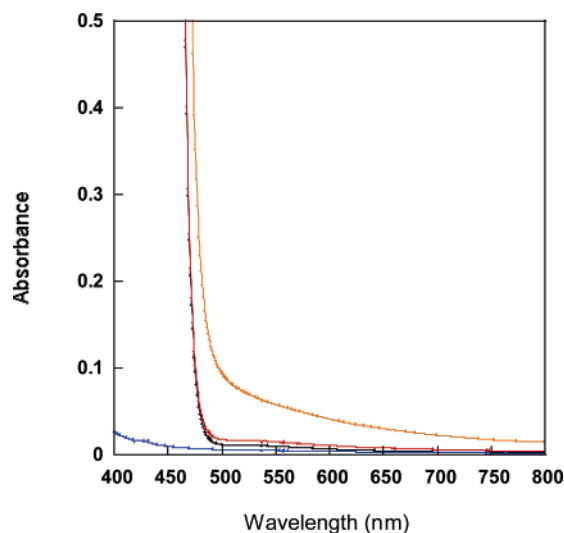


**Figure 9.** UV-vis absorption spectra of  $\text{CH}_3\text{CN}$  solutions of  $\mathbf{1}\cdot(\text{OTf})_4$  (concentration = 2.0 mM, black) and Py (concentration = 8.0 mM, blue), the sum of the two spectra (red), and the mixture of  $\mathbf{1}\cdot(\text{OTf})_4$  and Py of the same concentrations (orange).

binds to  $\mathbf{1}^{4+}$ . In other words, the emission is not quenched by bimolecular (Stern–Volmer) reactions between  $\mathbf{1}\cdot(\text{OTf})_4$  and the aromatic molecules.

**Possible Quenching Mechanism.** The X-ray crystal structures of the inclusion complexes clearly show that the complexation alters the conformation of  $\mathbf{1}^{4+}$ . Particularly, the central ring in the anthracenyl undergoes severe out-of-plane distortion upon the binding. It is possible that the distortion affects the emission quantum yield ( $\Phi_{\text{em}}$ ) of the anthracenyl rings. Another plausible quenching mechanism is energy transfer from the anthracenyl  $\pi\pi^*$  excited state to a nonemitting charge-transfer (CT) excited state which arises from the interactions between the bipy and the guest. Previous studies showed that the fluorescence of anthracene<sup>56</sup> and hydroquinols<sup>36c</sup> is quenched upon their binding to the  $\text{CBPQT}^{4+}$  ion. The UV-vis absorption spectra of the inclusion complexes exhibit low-energy charge-transfer absorption bands ascribable to the electronic transition from the  $\pi$ -electron-rich guests to the  $\pi$ -electron-deficient bipyridinium in  $\text{CBPQT}^{4+}$ .<sup>36,56</sup> The quenching is attributed to fast energy transfer from the emitting  $\pi\pi^*$  excited state of the guest to the low-lying CT excited state, which returns to the ground state via radiationless decay. While the UV-vis absorption spectra of  $\text{CH}_3\text{CN}$  solutions which contain  $\mathbf{1}\cdot(\text{OTf})_4$  and excess guests show no distinct new absorption band, a weak absorption tailing from 500 to 800 nm is observed in the spectra of the mixtures of  $\mathbf{1}\cdot(\text{OTf})_4$  and Nap, Phen, An, Br–An,  $\text{CO}_2\text{H}$ –An (Figures S66–70), and Py. No such absorption tail is found in the sum of the spectra of  $\mathbf{1}\cdot(\text{OTf})_4$  and the guests recorded at the same concentrations. Figure 9 shows the absorption spectra of the mixture of  $\mathbf{1}\cdot(\text{OTf})_4$  and Py, and the sum of the spectra of the two compounds. Similar absorption spanning ~500–700 nm is observed in the solid-state UV-vis reflectance spectra of the crystals of the An-, Br–An-, and Py-complexes (Figure S71). The solids of  $\mathbf{1}\cdot(\text{OTf})_4$  do not display such an absorption tail which could be part of a CT band that overlaps with the absorption of the host and the guest. Notably, there is large overlap between the supposed CT absorption and the

emission of  $\mathbf{1}^{4+}$ , which would facilitate energy transfer from the excited state of  $\mathbf{1}^{4+}$  to the CT excited state. The CT excited state, believed to be nonemitting, would relax to the ground state via radiationless decay. The absence of similar CT absorption in the spectra of the mixtures of  $\mathbf{1}\cdot(\text{OTf})_4$  and excess Dmb and Bip could account for the fact that the two compounds do not quench the emission.

**Apparent Quenching of the Guests.** The emission intensity of all of the guests is reduced upon addition of  $\mathbf{1}\cdot(\text{OTf})_4$  to the  $\text{CH}_3\text{CN}$  solutions of the compounds. The decrease in the emission intensity of the guests is found to obey the Beer's Law, showing linear plots of  $\log I_G^0/I_G$  versus  $[H]_t$  ( $I_G$  and  $I_G^0$  are the emission intensity of the guests in the presence and absence of  $\mathbf{1}^{4+}$ , respectively). Furthermore, the gradients of the plots are equal to the extinction coefficients of  $\mathbf{1}^{4+}$  (Figures S72–76). In other words, the  $\mathbf{1}^{4+}$  ion, acting like an emission filter, attenuates the fluorescence intensity of the guests by absorbing the emitted light. The filter effect is due to the extensive overlap between the intense low-energy  $\pi \rightarrow \pi^*$  absorption band of  $\mathbf{1}^{4+}$ , which ranges from 320 to 480 nm, and the fluorescence of the guests. Nonetheless, it does not necessarily rule out quenching of the guests by processes such as intramolecular energy transfer to the CT excited state. It is because the absorption of the host is so dominating that it is virtually impossible to extract the binding constants from the titrations.

**Stability of the Inclusion Complexes.** The structural and spectroscopic results clearly show that the complexation between  $\mathbf{1}^{4+}$  and the guests is predominantly resulted from the interactions between the aromatic rings of the host and the guests. In addition, the edge-to-face interactions could contribute to the stability of the inclusion complexes containing the “long” guests such as An and Py. In fact, the binding of the guests to  $\mathbf{1}^{4+}$  belongs to a class of host–guest complexation which involves receptors with permanent charge and neutral aromatic molecules.<sup>57</sup> A multitude of secondary interactions including van der Waal, charge-transfer (CT), solvophobic effect,<sup>58</sup> and electrostatic interactions have been invoked as the driving forces of this class of complexation.

The common way to probe the driving forces of the complexation is to correlate the free energy of binding with different molecular properties of the guests and other physical quantities.<sup>58,59</sup> CT interactions have been suggested to be responsible for the complexation between  $\text{CBPQT}^{4+}$  and electron-rich aromatic molecules.<sup>36a,b,60</sup> It is supported by the correlation between the free energy of binding and the electron-donating ability of the guests.<sup>60</sup> Furthermore, for the complexation between  $\text{CBPQT}^{4+}$  and tetrathiafulvalene and its derivatives (TTF), the free energy of binding is increased as the reduction potential of TTF is decreased.<sup>60c</sup> However, the plot

(56) Ballardini, R.; Balzani, V.; Dehaen, W.; Dell'Erba, A. E.; Raymo, F. M.; Stoddart, J. F.; Venturi, M. *Eur. J. Org. Chem.* **2000**, 591.

(57) (a) Schneider, H.-J.; Mohammad-Ali, A. K. Receptors for Organic Guest Molecules. In *Comprehensive Supramolecular Chemistry*; Lehn J.-M., Chair Ed.; Atwood, J. L., Davis, J. E. D., MacNicol, D. D., Vögtle, F., Exec. Eds.; Pergamon: Oxford, UK, 1996; Vol. 3, Chapter 3. (b) Diederich, F. *Angew. Chem., Int. Ed. Engl.* **1988**, *27*, 362.

(58) (a) Schneider, H.-J.; Kramer, R.; Simova, S.; Schneider, U. *J. Am. Chem. Soc.* **1988**, *110*, 6442. (b) Ferguson, S. B.; Sandford, E. M.; Seward, E. M.; Diederich, F. *J. Am. Chem. Soc.* **1991**, *113*, 5410. (c) Mirzozian, A.; Kaifer, A. E. *J. Org. Chem.* **1995**, *60*, 8093. (d) Liu, T.; Schneider, H.-J. *Angew. Chem., Int. Ed.* **2002**, *41*, 1368.

(59) (a) Schneider, H.-J.; Juneja, R. K.; Simova, S. *Chem. Ber.* **1989**, *122*, 1211. (b) Cancaill, J.; Cesario, M.; Collet, A.; Guilhem, J.; Lacombe, L.; Lozach, B.; Pascard, C. *Angew. Chem., Int. Ed. Engl.* **1989**, *28*, 1246. (c) Smithrud, D.; Diederich, F. *J. Am. Chem. Soc.* **1990**, *112*, 339.

of  $-\Delta G_{\text{NMR}}$  versus the reported reduction potentials of the guests<sup>61</sup> measured in  $\text{CH}_3\text{CN}$  ( $\text{Guest}^+ + 1e^- \rightarrow \text{Guest}^0$ ,  $E$  vs SCE) (Figure 10a and Table 6) shows no correlation, implying that the CT interactions are not the primary driving force for the guest binding to  $\mathbf{1}^{4+}$ . This conclusion does not contradict with the observation of CT absorption bands in the solutions and solids of the inclusion complexes. In fact, studies showed that the CT interactions between some aromatic donors and acceptors can be very weak even though the mixtures of the compounds display CT bands in the UV-vis spectra.<sup>62</sup>

As the guests are transferred from a solvent cage to the cavity of  $\mathbf{1}^{4+}$  upon complexation, their interactions with the solvent could affect the binding strength. The affinity of the guests for the solvent can be gauged by their solubility, which can be determined by the UV-vis spectrometric method (Table 6). The complexation also leads to the displacement of solvent molecules from the cavity of  $\mathbf{1}^{4+}$ , which also requires free energy. Assuming this free energy is similar for the binding of all of the guests, one would expect a correlation between the solubility of the guests and the  $-\Delta G_{\text{NMR}}$  if the solvophobic effect is one of the main driving forces of the complexation.<sup>58</sup> Our analysis shows that the correlation of  $-\Delta G_{\text{NMR}}$  and the solubility of the guests is reasonably good ( $R = 0.93$ ) (Figure 10b). In general, the sparingly soluble polycyclic An, substituted An, Phen, and Py, bind more strongly to  $\mathbf{1}^{4+}$  than the more soluble Dmb, Bip, and Nap. This indicates that the solvophobic effect could be partly responsible for the stability of the inclusion complexes of the large aromatic molecules.

van der Waals interactions consist of dispersive forces and attractions that are due to dipole induced by permanent charges. Schneider et al. have shown that the binding of neutral aromatic guests to charged cyclophanes that contain a  $\pi$ -surface is markedly stronger than that to analogous cyclophanes which are neutral.<sup>63</sup> The increase in the binding strength has been attributed to the ion-dipole interactions between the charges in the cyclophane and the  $\pi$ -electrons of the guests. Notably, a study of the complexation between  $\text{CBPQT}^{4+}$  and disubstituted biphenyls and benzenes shows a good correlation between the binding free energy and the molecular polarizability of the guests.<sup>64</sup> The averaged molecular polarizability ( $\alpha_{\text{M}}$ ) of Nap, Phen, An, Br-An, and Py was reported.<sup>65</sup> On the other hand, the  $\alpha_{\text{M}}$  of Dmb, Bip, MeO-An, NC-An, and  $\text{CO}_2\text{H-An}$  can be estimated using Miller's empirical equation<sup>66</sup>  $\alpha_{\text{m}} = (4/N) [\sum_a \tau_a]^2$ , where  $N$  is the total of number of electrons in the molecule and  $\tau_a$  is the parametrized polarizability of individual atoms in the molecule (Table 6). As expected from their higher number of  $\pi$ -electrons, the large aromatic molecules like Py and An, are more polarizable than the smaller and less

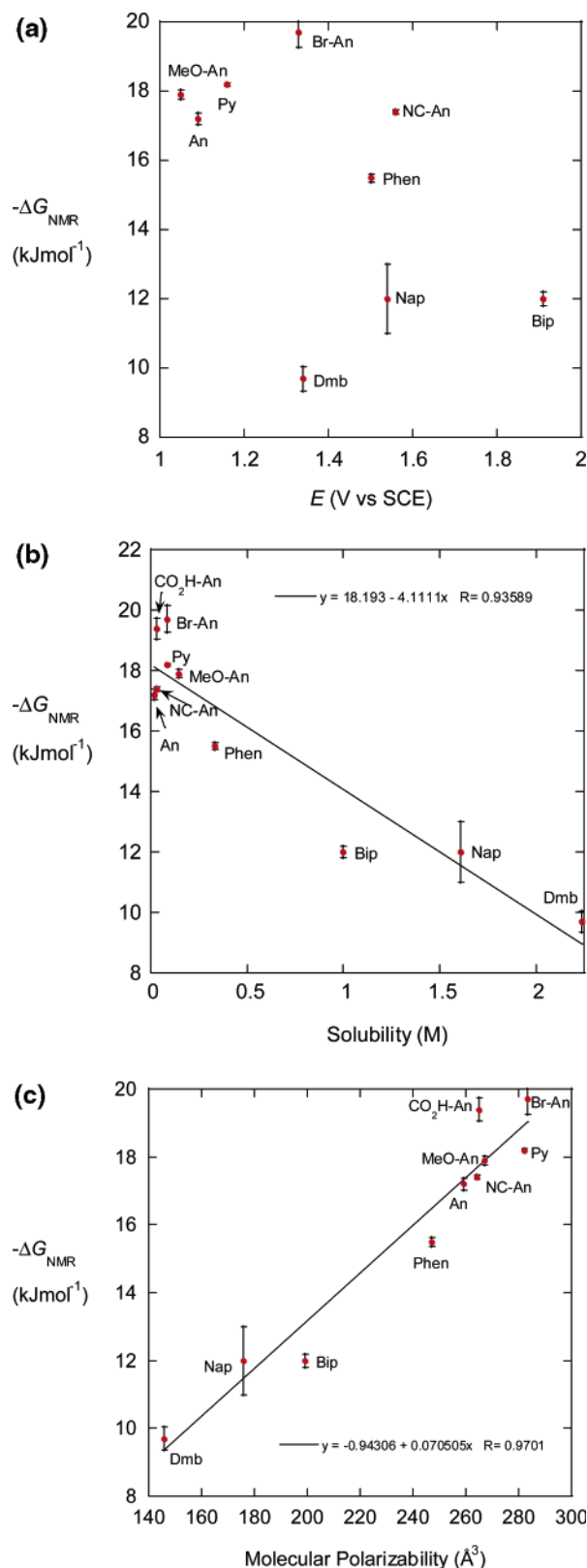


**Figure 10.** Plots of  $-\Delta G_{\text{NMR}}$  versus (a) oxidation potentials, (b) solubility, and (c) molecular polarizability of the guests.

conjugated Dmb, Bip, and Nap. The plot of  $-\Delta G_{\text{NMR}}$  versus the  $\alpha_{\text{M}}$  of the guests shows a reasonably good correlation with  $R = 0.97$  (Figure 10c). This suggests that the higher binding affinity exhibited by the large aromatic molecules is partly due to the increased ion-dipole interactions.

- (60) (a) Goodnow, T. T.; Reddington, M. V.; Stoddart, J. F.; Kaifer, A. E. *J. Am. Chem. Soc.* **1991**, *113*, 4335. (b) Bernardo, A. R.; Stoddart, J. F.; Kaifer, A. F. *J. Am. Chem. Soc.* **1992**, *114*, 10624. (c) Nielsen, M. B.; Jeppesen, J. O.; Lau, J.; Lomholt, C.; Damgaard, D.; Jacobsen, J. P.; Becher, J.; Stoddart, J. F. *J. Org. Chem.* **2001**, *66*, 3559.
- (61) *CRC Handbook Series in Organic Electrochemistry*; Meites, L.; Zuman, P., Eds.; CRC Press: Cleveland, OH, 1976–1993; Vols. 1–6.
- (62) Diederich, F.; Philip, D.; Seiler, P. *J. Chem. Soc., Chem. Commun.* **1994**, 205.
- (63) (a) Schneider, H.-J.; Blatter, T.; Simova, S.; Theis, I. *J. Chem. Soc., Chem. Commun.* **1989**, 580. (b) Schneider, H.-J.; Blatter, T. *Angew. Chem., Int. Ed. Engl.* **1988**, *27*, 1163.
- (64) Castro, R.; Berardi, M. J.; Cordova, E.; Ochoa de Olza, M.; Kaifer, A. E.; Evansck, J. D. *J. Am. Chem. Soc.* **1996**, *118*, 10257.
- (65) *CRC Handbook of Chemistry and Physics*, 84th ed.; Lide, D. R., Chair Ed.; CRC Press: Cleveland, OH, 2003.
- (66) Miller, K. J. *J. Am. Chem. Soc.* **1990**, *112*, 8533.

**Table 6.** Binding Free Energy, Solubility, Molecular Polarizability, and Oxidation Potential of the Guests

| guests               | $-\Delta G_{\text{NMR}}$ (kJ mol <sup>-1</sup> ) | solubility (M) | molecular polarizability $\alpha_{\text{M}}$ (Å <sup>3</sup> ) | $E$ (V vs SCE) <sup>c</sup> |
|----------------------|--|----------------|--|-----------------------------|
| Dmb                  | 9.7 ± 0.4  | 2.420          | 146.0 <sup>b</sup>   | 1.34                        |
| Bip                  | 12.0 ± 0.2                                       | 1.030          | 199.0 <sup>b</sup>   | 1.91                        |
| Nap                  | 12.0 ± 1.0                                       | 1.602          | 175.9 <sup>a</sup>   | 1.54                        |
| Phen                 | 15.5 ± 0.1                                       | 0.310          | 247.0 <sup>a</sup>   | 1.50                        |
| An                   | 17.2 ± 0.2                                       | 0.020          | 259.3 <sup>a</sup>   | 1.09                        |
| MeO-An               | 17.9 ± 0.1                                       | 0.150          | 267.2 <sup>b</sup>   | 1.05                        |
| NC-An                | 17.4 ± 0.1                                       | 0.033          | 264.3 <sup>b</sup>   | 1.56                        |
| Br-An                | 19.7 ± 0.4                                       | 0.085          | 283.2 <sup>a</sup>   | 1.33                        |
| CO <sub>2</sub> H-An | 19.4 ± 0.3                                       | 0.031          | 264.9 <sup>b</sup>   |                             |
| Py                   | 18.2 ± 0.1                                       | 0.082          | 282.2 <sup>a</sup>   | 1.16                        |

<sup>a</sup> Reference 65. <sup>b</sup> The molecular polarizability of the compounds is calculated from the empirical formula  $\alpha_{\text{m}} = (4/N)[\sum_a \tau_a]^2$ , where  $N$  is the total of number of electrons in the molecule and  $\tau_a$  is the parametrized polarizability of individual atoms in the molecule.<sup>66</sup> <sup>c</sup> All of the potentials cited are half-wave potentials measured in CH<sub>3</sub>CN, except for that for Bip which is the peak potential (ref 61).

## Conclusions

To summarize, we have demonstrated the facile synthesis of a kinetically stable nanoscopic luminescent gold rectangle by the self-assembly between the di-gold(I) clip Au<sub>2</sub>( $\mu$ -PAnP)(X)<sub>2</sub> (X = NO<sub>3</sub><sup>-</sup> or OTf<sup>-</sup>) and 4,4-bipyridine. The molecular recognitions of the gold rectangles in the solid state and solution have been studied in detail. It has been shown that the molecular rectangles assemble into 2D mosaic in the solid state via the complementary edge-to-face Ph-Ph interactions in the solid state. <sup>1</sup>H NMR and fluorescence titrations, along with the structural results, showed that the gold rectangle is a receptor for aromatic molecules of different sizes and electronic properties. The X-ray crystal structures of the inclusion complexes

show the presence of  $\pi$ - $\pi$  interactions between the guests and the bipy and edge-to-face or C-H $\cdots\pi$  bonding between the guests and the anthracenyl backbones of the host. Comparing the structures of the inclusion complexes suggests the manifestation of an induced-fit mechanism in the complexation. The fluorescence of the gold rectangle is quenched upon the guest binding. It has been argued that the quenching is due to either structural changes of the gold rectangle triggered by the guest binding or fast energy transfer from the emitting excited state of the gold rectangle to the nonemitting CT excited state. Finally, the higher binding affinity exhibited by the polycyclic aromatic guests is related to the solvophobic effect, ion-dipole interactions, and the edge-to-face interactions.

**Acknowledgment.** This work is dedicated to Professor Sunney I. Chan on the occasion of his retirement. We thank Ms. Tan Geok Kheng for her assistance in the determinations of the X-ray crystal structures. We also thank the National University of Singapore for financial support.

**Supporting Information Available:** Synthesis and characterizations, X-ray crystallography data, ESI-MS, calculated isotopic distributions, cyclic voltamograms of the free ligands, packing of the An and Py complexes, <sup>1</sup>H NMR titrations, modified Job's plots, titration curve fittings, fluorescence titrations and curve fittings, charge-transfer absorption spectra, Beer's plots of the absorption of the guest emission by the host, and CIF files of Au<sub>2</sub>( $\mu$ -PAnP)(NO<sub>3</sub>)<sub>2</sub>·0.5Et<sub>2</sub>O, **1**·(OTf)<sub>4</sub>·4.8H<sub>2</sub>O, (**1**⊃An)·(OTf)<sub>4</sub>, (**1**⊃Py)·(OTf)<sub>4</sub>·CH<sub>2</sub>Cl<sub>2</sub>, and (**1**⊃Br-An) (OTf)<sub>4</sub>·Et<sub>2</sub>O. This material is available free of charge via the Internet at <http://pubs.acs.org>.

JA0456508